Biochimica et Biophysica Acta 1798 (2010) 401–414

Contents lists available at ScienceDirect

Biochimica et Biophysica Acta

journal homepage: www.elsevier.com/locate/bbamem

Interaction with membrane mimics of transmembrane fragments 16 and 17 from the human multidrug resistance ABC transporter 1 (hMRP1/ABCC1) and two of their tryptophan variants

Béatrice de Foresta [a,b,*], Michel Vincent [c], Jacques Gallay [c], Manuel Garrigos [a,b]

[a] CEA, iBiTecS, SB²SM, F-91191, Gif-sur-Yvette, France
[b] CNRS, URA 2096, F-91191, Gif-sur-Yvette, France
[c] Institut de Biochimie et de Biophysique Moléculaire et Cellulaire, Université Paris-Sud, UMR8619-CNRS, IFR115, F-91405 Orsay, France

ARTICLE INFO

Article history:
Received 6 July 2009
Received in revised form 12 November 2009
Accepted 30 November 2009
Available online 11 December 2009

Keywords:
hMRP1 (ABCC1)
Multidrug resistance
TM fragments
Steady-state and time-resolved fluorescence
Brominated detergents
Dodecylmaltoside
Dodecylphosphocholine micelles

ABSTRACT

The human multidrug resistance-associated protein 1 (hMRP1/ABCC1) belongs to the ATP-binding cassette transporter superfamily. Together with P-glycoprotein (ABCB1) and the breast cancer resistance protein (BCRP/ABCG2), hMRP1 confers resistance to a large number of structurally diverse drugs. The current topological model of hMRP1 includes two cytosolic nucleotide-binding domains and 17 putative transmembrane (TM) helices forming three membrane-spanning domains. Mutagenesis and labeling studies have shown TM16 and TM17 to be important for function. We characterized the insertion of the TM16 fragment into dodecylphosphocholine (DPC) or *n*-dodecyl-β-D-maltoside (DM) micelles as membrane mimics and extended our previous work on TM17 (Vincent et al., 2007, *Biochim. Biophys. Acta* 1768, 538). We synthesized TM16 and TM17, with the Trp residues, W1198 in TM16 and W1246 in TM17, acting as an intrinsic fluorescent probe, and TM16 and TM17 Trp variants, to probe different positions in the peptide sequence. We assessed the interaction of peptides with membrane mimics by evaluating the increase in fluorescence intensity resulting from such interactions. In all micelle-bound peptides, the tryptophan residue appeared to be located, on average, in the head group micelle region, as shown by its fluorescence spectrum. Each tryptophan residue was partially accessible to both acrylamide and the brominated acyl chains of two DM analogs, as shown by fluorescence quenching. Tryptophan fluorescence lifetimes were found to depend on the position of the tryptophan residue in the various peptides, probably reflecting differences in local structures. Far UV CD spectra showed that TM16 contained significant β-strand structures. Together with the high Trp correlation times, the presence of these structures suggests that TM16 self-association may occur at the interface. In conclusion, this experimental study suggests an interfacial location for both TM16 and TM17 in membrane mimics. In terms of overall hMRP1 structure, the experimentally demonstrated amphipathic properties of these TM are consistent with a role in the lining of an at least partly hydrophilic transport pore, as suggested by the currently accepted structural model, the final structure being modified by interaction with other TM helices.

Abbreviations: hMRP1 (or ABCC1), human multidrug resistance protein 1; BCRP (or ABCG2), breast cancer resistance protein; LTC_4, cysteinyl leukotriene C_4; $E_2$17βG, estradiol 17-(β-D-glucuronide); GSH, reduced glutathione; DM, *n*-dodecyl-β-D-maltoside; BrDM, 7, 8-dibromododecylmaltoside; BrUM, 10, 11-dibromoundecanoylmaltoside; DPC, dodecylphosphocholine; cmc, critical micellar concentration; NATA, *N*-acetyltryptophanamide; TOE, tryptophan octyl ester; DMSO, dimethylsulfoxide; TFE, trifluoroethanol; TFA, trifluoroacetic acid; MSD, membrane-spanning domain; TM, transmembrane fragment; NBD, nucleotide-binding domain; MEM, maximum entropy method; CD, circular dichroism; FWHM, full-width at half-maximum; P3, $K_2WL_9AL_9K_2A$; P5, $K_2CLWL_7AL_9K_2A$; P7, $K_2CL_3WL_5AL_9K_2A$; P9, $K_2CL_5WL_3AL_9K_2A$; P11, $K_2CL_7WLAL_9K_2A$; P13, $K_2CL_9WL_9K_2A$; TM16, A_{1195}NRWLAVRLECVGNCIVLFAALFAV$_{1219}$; mTM16, A_{1195}NRWLAVRLESVGNSIVLFAALFAV$_{1219}$; W19-mTM16, A_{1195}NRYLAVRLESVGNSIVLWAALFAV$_{1219}$; TM17, A_{1227}GLVGLSVSYSLQVTTYLNWLVRMS$_{1251}$; mTM17, K_{1227}GLVGLSVSYSLQVTTYLNWLVRMS$_{1251}$; W10-mTM17, K_{1227}GLVGLSVSWSLQVTTYLNYLVRMS$_{1251}$

* Corresponding author. CEA, iBiTecS and CNRS, URA 2096, CEA Saclay, F-91191, Gif-sur-Yvette, France. Tel.: +33 1 69 08 89 44; fax: +33 1 69 08 81 39.
E-mail address: Beatrice.de-foresta@cea.fr (B. de Foresta).

0005-2736/$ – see front matter © 2009 Elsevier B.V. All rights reserved.
doi:10.1016/j.bbamem.2009.11.019

1. Introduction

The human ATP-binding cassette (ABC) transporter family consists of 48 integral membrane proteins that are involved in a variety of physiological processes based on the translocation of specific allocrites (transported compounds) across intracellular membranes or out of the cell [1]. The energy required to transport the allocrite across a membrane and against a concentration gradient is derived from the hydrolysis of ATP. Identified mutations in several ABC transporters are responsible of genetic diseases (cystic fibrosis, Tangier disease, Stargardt disease, etc.) [2]. According to phylogenetic analysis, the 48 ABC transporters are classified into seven distinct subfamilies of proteins named ABCA through ABCG [3]. The human multidrug resistance-associated protein 1 (hMRP1/ABCC1) was discovered in 1992 and cloned from a multidrug-resistant lung cancer cell line [4]. The hMRP1 represents the founding member of the ABCC subfamily which comprises 13 members (http://nutrigene.4t.com/humanabc.htm). It is expressed constitutively at moderate levels in most healthy tissues and is capable to transport a wide range of structurally unrelated molecules including amphiphilic anionic conjugates, such as glutathione (GSH)-, glucuronate-, and sulfate-conjugated aliphatic or heterocyclic compounds, across membranes [5–7]. hMRP1 also transports unconjugated drugs in the presence of GSH, likely through a cotransport mechanism [7–12]. Together with Pgp (ABCB1) [13] and the breast cancer resistance protein, BCRP (ABCG2/MXR) [14], hMRP1 is associated with the multidrug resistance phenotype (MDR) [15–17]. The hMRP1 is highly expressed in many drug-resistant solid tumors like in lung, breast, and prostate cancers and most probably represents a major obstacle to successful chemotherapy in lung cancer [6]. Moreover, the fact that substances of toxicological relevance are transported by hMRP1 together with its constitutive expression in biological barriers like the blood–brain barrier suggests it might play a role in defence against xenobiotics.

hMRP1 is a large glycosylated integral membrane protein with an M_r of 190,000 (1531 residues). According to protein folding algorithms, it contains three membrane-spanning domains (MSD). The current topological model (Scheme 1), which is supported by epitope insertion [18,19] and glycosylation site mutation data [20], includes a specific N-terminal domain, MSD0, preceded by an extracytosolic N-terminus and followed by a cytosolic loop (L0), together with two membrane domains MSD1 and MSD2, each followed by a nucleotide-binding domain (NBD). Five transmembrane (TM) helices are predicted for MSD0, whereas MSD1 and MSD2 each consist of six TM fragments. With the exception of MSD0, this topology is that generally shared by other human ABC full transporters [21].

High-resolution crystal structures have recently been determined for ABC transporters from four microorganisms [22]. Two of these transporters were exporters, like hMRP1: the bacterial lipid transporter MsBA (the published structure of which has since been retracted [23]) and the Sav1866 transporter from *Staphylococcus aureus*, crystallized in two conformations [24,25]. Models of hMRP1 MSD1 and MSD2 have been proposed on the basis of these structures [5,26,27]. However, the transmembrane segments of these proteins differ much more than their nucleotide-binding domains, due to differences in substrate specificity, so complementary structural approaches are still informative in the absence of a crystal structure for hMRP1.

Investigation of the structural properties of membrane proteins through studies of isolated transmembrane fragments is a widely recognized approach (e.g., [28,29]). It is based on a two-stage model [30,31], partly arising from bacteriorhodopsin refolding studies [32], and suggesting that the folding of membrane proteins includes an initial step during which independently stable transmembrane helices are formed and further associate within the membrane. A more comprehensive view includes additional stages, such as helix–helix association, leading to further folding events [33]. Initial events, such as the interfacial binding and folding of a TM fragment, have also been rationalized from a thermodynamic viewpoint [34]. The way the proteins are inserted in membranes *in vivo*, via their interaction with the translocon, also begins to be better understood [35,36].

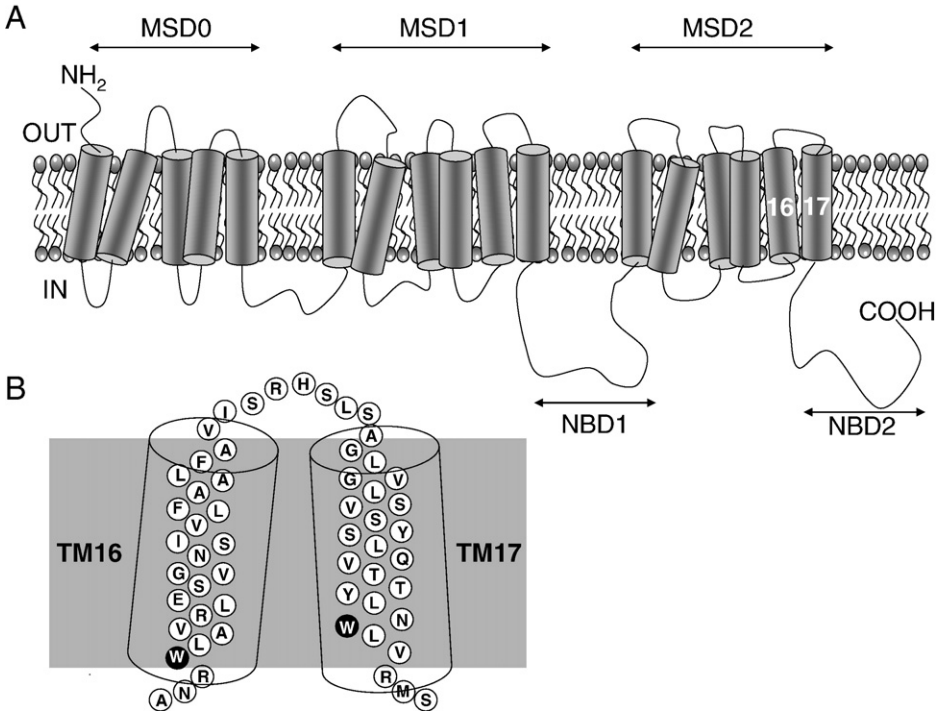

Scheme 1. Topology of hMRP1 membrane transporter. (A) Functional unit of hMRP1 containing three membrane-spanning domains (MSD) and two nucleotide-binding domains (NBD). (B) Isolated sequences of the putative transmembrane TM16 and TM17 fragments with their corresponding tryptophan residues highlighted in black circles.

We recently studied the overall structure, dynamics and location of TM17—the last transmembrane fragment of hMRP1—in membrane mimetic systems, by means of Trp fluorescence and far UV circular dichroism [37]. We chose to study this segment, because some of its polar amino acid residues, including its single-Trp1246 residue, have been shown to be important for the function of the protein, particularly as concerns the transport of estradiol 17-(β-D-glucuronide), an endogenous metabolite [38,39]. Molecular modeling of MSD1 and MSD2 has suggested that TM17 was part of the transmembrane transport pore, as well in the initial model of this pore [26] as in the recent model that includes a larger number of TM segments [27]. Our results were consistent with an interfacial location of this fragment in the DPC and DM micelles used as membrane mimics, as shown by both the shallower position of the Trp in the mixed peptide-detergent micelles than in the single-Trp model transmembrane peptides studied in the same conditions [37,40] and by the only partial structuring of the peptide into an α-helix. We therefore suggested that additional factors, such as interactions with other TM, were required to maintain TM17 in a transmembrane position.

In this work, we extended this approach to the TM fragment preceding TM17 in hMRP1, TM16, and added to our previous results, using new synthetic peptides for TM17 (Table 1). TM16 is a good candidate for interaction with TM17, because these two segments are linked together in the protein by a short loop of few residues, located between V1219 and A1227, in the various TM structure predictions (Scheme 1). Site-directed mutagenesis experiments have also indicated that the ionizable residues of TM16, Arg1197, Arg1202, and Glu1204, play a crucial role in protein expression, substrate binding, and/or transport [41]. These residues are strongly conserved in the ABCC family. TM16 also contains a single tryptophan residue, Trp1198, located on the cytoplasmic side of the protein, like the Trp1246 residue of TM17, and involved in overall transport activity [42]. The intracellular loop between TM15 and TM16 also plays a key role in transport, mostly mediated by its charged amino acids, some of which are proximal to the TM16 N-terminus (Asp1179, Lys1181, and Asp1183) [43–46]. The choice of appropriate fragments for study is a key issue. For this study, we synthesized a Cys1205Ser and Cys1209Ser double mutant of TM16 (mTM16), containing a single-Trp residue, W1198, close to the N-terminus (or W4 in the peptide sequence) (Table 1). The replacement of these Cys residues had no effect on substrate specificity or transport activity [47]. We synthesized a TM16 Trp variant (W19-mTM16), in which the aromatic residue Phe1213 was replaced by a tryptophan residue, to probe a part of TM16 closer to the C-terminus (i.e., to the extracellular side in the whole protein). The conservative substitution of Trp1198 in hMRP1 allows the protein to preserve its transport activity [42]. Similarly, a Ala1227Lys mutant of the TM17 fragment (mTM17) containing Trp1246 (or W20) [37] and the Tyr1236Trp and Trp1246Tyr variant of mTM17 (W10-mTM17), with its Trp closer to the extracellular side in the whole protein, were also synthesized (Table 1).

As previously [37,40,48], detergent micelles were chosen as membrane mimics because they allow easier solubilization of such amphipathic peptides and that the artefacts linked to light absorption and scattering are minimized with respect to membrane models such as lipid vesicles. Among various suitable detergents, DM, a neutral detergent, was specifically chosen, in particular because we developed the use of DM-brominated analogs to study Trp location in micelles from fluorescence quenching [37,40,48]. The zwitterionic DPC was also chosen here because it generates an interfacial region very similar to that generated by phospholipids [49,50] and favors the structuring of amphipathic peptides (e.g., [37,48]).

After assessing peptide binding to detergent micelles, we studied the peptide–detergent complexes in steady-state and time-resolved Trp fluorescence experiments, including quenching with acrylamide and brominated analogs of DM. These experiments provided information about the Trp microenvironment, its accessibility to quenchers, its conformer equilibrium and dynamics (subnanosecond and nanosecond time ranges). The secondary structure of TM16 in various media was assessed by far UV circular dichroism and compared to that obtained for TM17 [37]. Consistent with our previous observations, both TM16 and TM17 seemed to have an interfacial location, which we considered to be related to the specialization of hMRP1 in the transport of polar substrates.

2. Materials and methods

2.1. Chemicals

n-Dodecyl-β-D-maltoside (DM) was obtained from Calbiochem. Two brominated derivatives, 7,8-dibromododecylmaltoside (BrDM) and 10,11-dibromoundecanoylmaltoside (BrUM), were synthesized by Insavalor (Villeurbanne, France), as previously described [51,52]. DPC was obtained from Anatrace (OH, USA). Stock solutions of these detergents were prepared in Milli-Q water at concentrations of 100 or 200 mM. *N*-acetyltryptophanamide (NATA) and acrylamide were purchased from Sigma-Aldrich. We made up a stock solution of 5 M acrylamide in water. Methanol, ethanol, DMSO (Uvasol quality), and TFE (for synthesis) were obtained from Merck. Buffers were filtered through Millex-HA filters (0.45 μm pore size; Millipore).

2.2. Peptide synthesis

Four 25-amino acid peptides were synthesized as trifluoroacetate salts by Jerini (Berlin, Germany), as shown in Table 1: (1) a peptide, referred to as mTM16 ($M_w = 2757$), encompassing the predicted

Table 1
Sequences of the four (25-amino acid) synthetic peptides and of the corresponding wild-type TM16 and TM17 of hMRP1.

Peptide name	Amino-acid sequence	Charge	ΔG_u[a]
TM16	A_{1195}NR**W**LAVRLECVGNCIVLFAALFAV$_{1219}$	++,−	−4.07
mTM16[b]	Ac-A_{1195}NR**W**LAVRLESVGNSIVLFAALFAV$_{1219}$-Am	++,−	−3.33
W19-mTM16	Ac-A_{1195}NRYLAVRLESVGNSIVL**W**AALFAV$_{1219}$-Am	++,−	−3.14
TM17	A_{1227}GLVGLSVSYSLQVTTYLN**W**LVRMS$_{1251}$	+	−6.23
mTM17[c]	Ac-K_{1227}GLVGLSVSYSLQVTTYLN**W**LVRMS$_{1251}$-Am	++	−5.41
W10-mTM17	Ac-K_{1227}GLVGLSVS**W**SLQVTTYLNYLVRMS$_{1251}$-Am	++	−5.41

The tryptophan residue used as an intrinsic fluorescent probe is shown in bold characters.

[a] Interfacial partitioning free energy for unstructured peptide, calculated with MPEX 3.0, for partition from water to bilayer, for the N-terminal-acetylated and C-terminal-amidated peptide.

[b] Sequence consistent with the prediction of Kast and Gros [19], with TM16 located between residues 1195 and 1220. mTM16 sequence also encompasses the more restrictive TM16 models N1196-A1218 [41] and W1198-A1218 [118], but is slightly extended at the N-terminal end, providing a native environment for Trp1198. The two wild-type Cys residues have been replaced by two Ser residues.

[c] *K* replaces A1227 to increase peptide solubility [37].

transmembrane fragment 16 of MRP1, except that the two native Cys residues, Cys1205 and Cys1209, were replaced by a Ser residue (the amino acid sequence numbering corresponding to the full-length published sequence of human MRP1 (GenBank accession no. 2828206); (2) a double mutant of this peptide (called W19-mTM16) ($M_w = 2774$), in which the position of the single Trp was changed, by two conservative substitutions, of the Trp1198 and Phe1213 residues, which were replaced by Tyr and Trp, respectively; (3) a peptide referred to as mTM17 ($M_w = 2855$), as in our previous study [37], encompassing the predicted transmembrane fragment 17 of MRP1, except that Ala1 was replaced by Lys; and (4) a double mutant of this peptide (W10-mTM17) ($M_w = 2856$), in which the position of the single Trp was changed, by two conservative substitutions, of Trp1246 and Tyr1236, which were replaced by Tyr and Trp, respectively. These peptides were acetylated at the N-terminus and amidated at the C-terminus. mTM16 and mTM17 were delivered at a purity of >80–90% whereas W19-TM16 and W10-TM17 were delivered at a purity of >85–90%, according to matrix-assisted laser desorption ionization time-of-flight (MALDI/TOF) mass spectrometry or HPLC-MS. These peptides were used as supplied.

2.3. Peptide solubilization assays and preparation of mixed peptide–detergent micelles

Transmembrane fragments are generally difficult to handle and solvents for stock solutions must be chosen carefully to prevent irreversible aggregation. mTM16 was not soluble in methanol, in contrast to mTM17, but could be dissolved in TFE. TFE was also a suitable solvent for the other peptides and was therefore used for peptide stock solutions in all cases (at usually 1 mM peptide).

The peptide concentrations obtained from weight measurements and absorption spectra in TFE gave values within ~15%. Taking into account the peptide composition (Table 1) and using molar absorption coefficients (at 280 nm) $\varepsilon = 5600\ M^{-1}\ cm^{-1}$ and $1400\ M^{-1}\ cm^{-1}$ for Trp and Tyr (Phe absorption at 280 nm being negligible), respectively, the molar absorption coefficients of the peptides were estimated as $\varepsilon_{max} = 5600$ for mTM16, 7000 for W19-TM16, and $8400\ M^{-1}\ cm^{-1}$ for both mTM17 and W10-mTM17, at the maximum absorption wavelength (~282 nm in TFE).

For fluorescence measurements, the mixed peptide–detergent micelles were generally prepared by adding an aliquot of the peptide stock solution to 10 mM potassium phosphate buffer, pH 7.5, at 20 °C, supplemented with 4 mM detergent (DM, DPC, or mixtures of DM with one of its brominated analogs), with a dilution factor of at least 100 and under constant stirring. In these conditions, most of DM and its analogs was in the micellar form, due to their low critical micellar concentrations (cmc) (170–180 μM, 220 μM, and 320 μM for DM, BrDM, and BrUM, respectively) [52,53]. For DPC, 2.9 mM (of 4 mM) detergent is micellar (as the cmc of DPC = 1.1 mM [50]).

2.4. Absorption measurements

Absorption spectra were recorded on an HP8453 diode array spectrophotometer, with a thermostatically controlled sample holder (20 °C). The sample was continuously stirred in a 1-cm path length cuvette.

2.5. Steady-state fluorescence measurements

Fluorescence data were obtained on a Spex Fluorolog spectrofluorimeter. The temperature in the cuvette was controlled with a thermostat and the sample was continuously stirred. We used standard quartz cuvettes (1 × 1 cm). Excitation spectra were corrected for the spectrum of the lamp and both excitation and emission spectra were corrected for fluctuations in lamp intensity (usually very small, <1%).

2.6. Spectral decomposition of steady-state fluorescence emission spectra

The steady-state fluorescence spectra were analyzed using up to two four-parameter log-normal functions (a skewed Gaussian equation) of the following form [54,55]:

$$I(\nu) = I_m exp\left\{-\left(ln2 / ln^2\rho\right) \times ln^2[(a-\nu)/(a-\nu_m)]\right\} \quad (\text{at } \nu < a)$$
$$I(\nu) = 0 \quad (\text{at } \nu \geq a)$$

Here, $I_m = I(\nu_m)$ is the maximal fluorescence intensity; ν_m is the wave number of the band maximum (peak); $\rho = (\nu_m - \nu_-)/(\nu_+ - \nu_m)$ is the band asymmetry parameter; ν_+ and ν_- are the wave number positions of left and right half-maximal amplitudes; a is the function-limiting point: $a = \nu_m + \text{FWHM}\ \rho/(\rho^2 - 1)$; the full width at half-maximum $\text{FWHM} = \nu_+ - \nu_-$.

We fitted a linear combination of this analytical model to the emission spectra by the least squares regression method (KaleidaGraph, Synergy Software, PA). A good fit was ensured by minimization of the squared residuals.

2.7. Fluorescence quenching by acrylamide

Fluorescence was quenched with acrylamide, as previously described [56]. Peptide quenching was analyzed using the classical Stern–Volmer equation (see, for reviews, [57]):

$$F_0 / F = 1 + K_{sv}[Q]$$

where F_0 and F are the fluorescence intensities in the absence and presence of quencher, respectively, K_{sv} is the Stern–Volmer quenching constant, and [Q] is the quencher concentration. K_{sv} is related to the bimolecular quenching constant k_q by the following formula:

$$K_{sv} = k_q \tau_0$$

where τ_0 is the lifetime, in the absence of quencher, of the fluorophore.

For NATA, taken as a reference, we used the nonlinear Stern–Volmer equation:

$$F_0 / F = (1 + K_{sv}[Q])\, exp V[Q]$$

where V can be considered as a sphere of action around the fluorophore in which the presence of a quencher molecule results in instantaneous (static) quenching.

2.8. Time-resolved fluorescence measurements

Fluorescence intensity and anisotropy decays were measured by the time-correlated single-photon counting technique from the polarized $I_{vv}(t)$ and $I_{vh}(t)$ components. They were performed as previously for mTM17, unless otherwise stated [37]. Briefly, a light-emitting diode (PLS 295, serial number PLS-8-2-237 from Picoquant, Berlin-Adlershof, Germany) (maximal emission at 298 nm) working at 10 MHz was used as an excitation source and a Hamamatsu photomultiplier (model R3235-01) was used for detection. The LED emission, focused with a UV lens, was filtered through a short-pass Asahi Spectra UV filter ZUS300. The fluorescence emission was collected through a 306AELP Omega long-pass filter and a UG11 Schott broad-band glass filter. The instrument response function was obtained at the excitation wavelength, with a glycogen scattering solution. As previously described, fluorescence intensity $I(t)$ and anisotropy decays $A(t)$ were analyzed as sums of 150 or 100 exponential terms, respectively, by the maximum entropy method (MEM) [58,59] according to the following equations:

$$I(t) = \sum \alpha_i exp(-t/\tau_i)$$

where α_i is the normalized amplitude and τ_i the excited state lifetime, and

$$A(t) = \sum \beta_i exp(-t/\theta_i)$$

where β_i is the anisotropy and θ_i the rotational correlation time. In this analysis, we assume that each lifetime τ_i is associated with all rotational correlation times θ_i [60]. The main advantage of MEM is that it does not impose any particular number of significant parameters for the decay. The Skilling–Jaynes entropy S was subjected to a χ^2 constraint [61] to ensure that the recovered distribution was consistent with the data.

2.9. Circular dichroism

Far UV circular dichroism spectra were recorded on a Jobin Yvon CD6 spectrodichrograph calibrated with ammonium d-10 camphorsulfonate. Measurements were made at 20 °C, using a 0. 1-cm path length quartz cuvette (Hellma) for 20 μM (or 25 μM) peptide in 10 mM potassium phosphate buffer, pH 7.5, with or without 4 mM detergent (DPC or DM). In TFE, peptide concentration was 100 μM in a 0. 01-mm path length cuvette. Spectra were recorded in the 185 to 250-nm wavelength range, with 0.5- nm wavelength increments, a 2-nm spectral bandwidth, and a 2- s integration time. Spectra were averaged over four scans and corrected for background. Unsmoothed spectra are presented.

Secondary structure was analyzed with the DICHROWEB Web server (http://dichroweb.cryst.bbk.ac.uk/html/home.shtml) [62,63]. Two different methods for analyzing protein CD spectra (CONTIN/LL and CDSSTR), two reference protein sets—set 3 (wavelength range: 185–240 nm, 37 proteins) and set 6 (wavelength range: 185–240 nm, 42 proteins)—and two scaling factors were tested. The CDSSTR method with protein set 6, using the mTM16 concentration determined by absorption, gave by far the most reliable analysis, as shown by the NRMSD (normalized root mean square deviation; range: 0.002–0.08) and comparison of the calculated and experimental spectra. This analysis was therefore used to evaluate mTM16 secondary structure.

3. Results

3.1. Binding of the TM16 and TM17 fragments to DM and DPC micelles

Each of the four fragments studied contained a single-Trp residue, the fluorescence of which provided information about the local properties of the peptide and of its local environment. Peptide–detergent interaction resulted in an increase in Trp fluorescence intensity, which was maximal for the W19-mTM16 fragment (see below). As an example, Fig. 1 shows the titration curve of W19-mTM16 fluorescence intensity as a function of detergent concentration (intensity measured at the maximum emission wavelength obtained in the presence of excess detergent). Significant peptide–detergent interaction was detected below the cmc of DPC (e.g., at 0.5 mM DPC), probably due to the interaction of detergent monomers with monomers or oligomers of this amphiphilic peptide, these oligomers forming rapidly in the absence of detergent micelles. Fluorescence continued to increase above the cmc of DPC (1.1 mM), to reach a plateau at ~2 mM detergent, a concentration at which no residual free peptide should be detected. Similar observations were recorded for DM, but with the binding curve shifted to lower detergent concentrations, due to the lower cmc of DM (~0.18 mM), and a smaller increase in fluorescence intensity. The other peptides behaved in a similar manner, but displayed a smaller increase in fluorescence intensity (not shown). All other fluorescence experiments were performed in the presence of excess detergent (4 mM) and the peptide was systematically added to the solution after the detergent, to prevent peptide oligomerization in buffer alone.

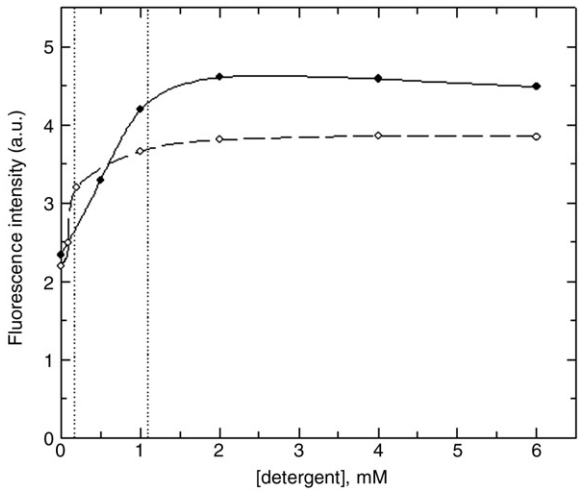

Fig. 1. Titration of the W19-mTM16 mutant with DPC and DM. We added 8 μM W19-mTM16 (circles) to 10 mM potassium phosphate buffer, pH 7.5, at 20 °C. Aliquots of DPC (closed symbols) or DM (open symbols) were then added sequentially, with continuous stirring, at constant intervals (~50 s). Fluorescence intensity was recorded continuously with λ_{ex} set at 280 nm. λ_{em} was set at 334 and 331 nm with DPC and DM, respectively. Slit widths were 1.25 mm (bandwidths ~5 nm) for both excitation and emission. The fluorescence intensities obtained after each addition of detergent were plotted as a function of total detergent concentration. DPC and DM cmcs are indicated as dotted lines.

3.2. Steady-state fluorescence spectra of TM16 and TM17 fragments in buffer, DM, and DPC

The fluorescence emission spectra of W4 in mTM16 and of W19 in the W19-mTM16 mutant, dispersed in buffer at micromolar concentrations from a stock solution in TFE, displayed maxima at 331–332 nm (Fig. 2A and B). By contrast to NATA, a model for a Trp completely accessible to the aqueous medium, which emits at ~353 nm in the same experimental conditions, this suggests that the Trp residues in these peptides were not fully exposed to the aqueous solvent, probably due to the formation of oligomers.

However, when diluted to the same concentrations in an excess of DM or DPC micelles in buffer, both peptides readily interacted with both detergent micelles, resulting in a significant increase in fluorescence intensity and a λ_{max} in the 331–335 nm range (Table 2). There was a striking difference between the two peptides in the presence of detergent micelles, with the fluorescence intensity recorded for W19-mTM16 (Fig. 1B) almost three times higher than that recorded for mTM16 (Fig. 1A). W19-mTM16 contains one Tyr residue in addition to its single-Trp residue (Table 1), but even efficient Tyr-Trp energy transfer could not account for such a large difference. Thus, for the peptides in detergent, the microenvironment or conformation of W19 must differ significantly from that of W4 and this difference should be evident in time-resolved fluorescence measurements. By contrast, the λ_{max} values of W4 and W19 were similar (within 1 nm) in all conditions.

Both peptides displayed a small but significant λ_{max} blue-shift (3 nm) in the presence of DM micelles with respect to DPC micelles. This blue-shift indicates that the Trp environment in DM micelles is slightly less polar than in DPC. The fluorescence emission spectra were decomposed further into elemental spectra, using log-normal Gaussian distributions [54,55,64,65]. In TFE, used as the reference, monomodal emission spectra were observed with a maximum at ~347 nm (not shown), indicating a homogeneous environment for Trp. By contrast, bimodal emission was observed for the fragments in both DM and DPC micelles (Table 2): a minor short-wavelength

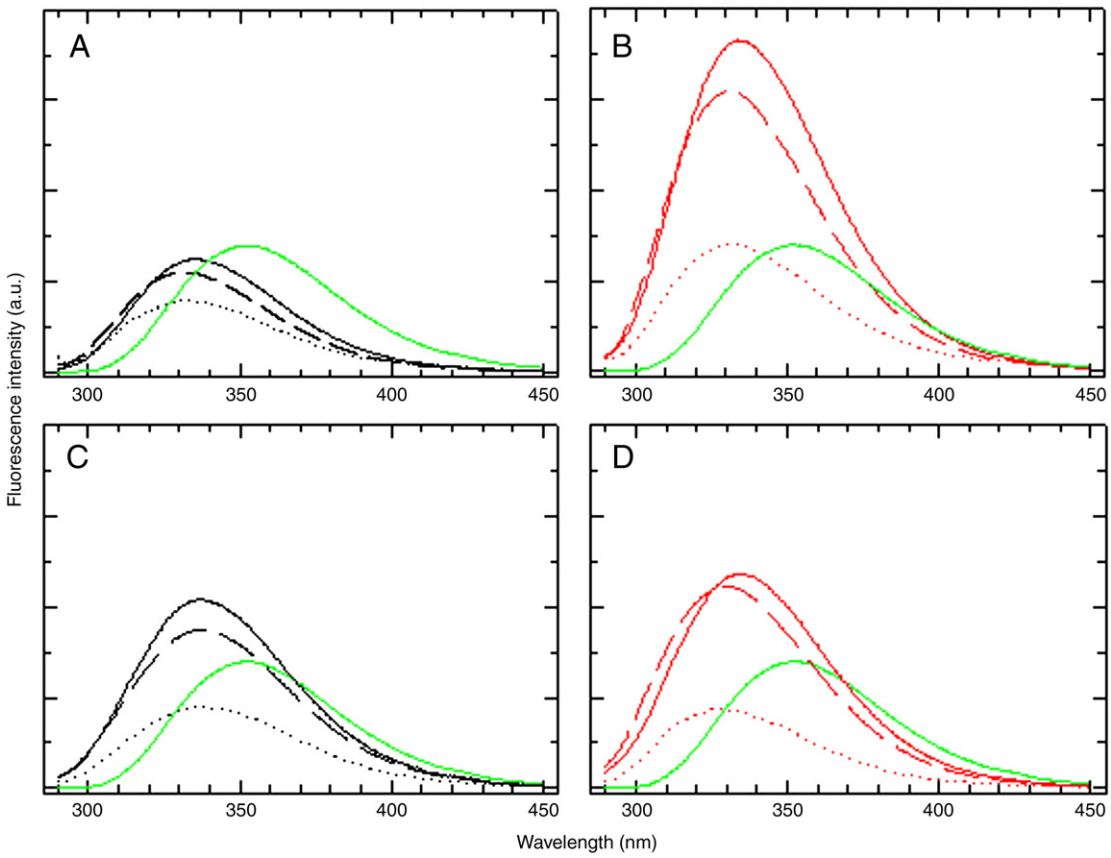

Fig. 2. Fluorescence emission spectra of the hMRP1 fragments in various media. (A and B) Emission spectra for 10 μM mTM16 (black lines) and W19-mTM16 (red lines) in 10 mM phosphate buffer, pH 7.5, alone (dotted line) or supplemented with 4 mM DPC (continuous line) or DM (dashed line), at 20 °C. λ_{ex} was set at 280 nm. Slit widths were 1.25 mm (bandwidths ~5 nm) for both excitation and emission. Spectra were recorded after a short period of equilibration (2–3 min), and the readings for background spectra (detergent in buffer) were subtracted. The emission spectrum of NATA in the same conditions is indicated as a reference (green line). (C and D) emission spectra for mTM17 (black lines) and W10-mTM17 (red lines), as in panel A and B.

spectrum (maximum ~321–326 nm) corresponding to roughly 34–39% of the raw spectrum and a major spectrum red-shifted by ~20 nm (maximum ~341–345 nm). These findings are consistent with a heterogeneous environment for the Trp residue.

Similar experiments were performed with W10-mTM17 and, for the sake of comparison, with mTM17 prepared as for the other fragments, from a stock solution in TFE. The emission spectra of these peptides in buffer and detergent micelles are shown in Fig. 2C and D. These fragments each contain a single-Trp and two-Tyr residues. Here again, the raw spectra are blue-shifted with respect to NATA, with λ_{max} values ranging from 328 to 337 nm, indicating partial Trp shielding from bulk water in all conditions. Higher fluorescence intensity values were recorded in the presence of detergent micelles. In detergent micelles, W10-mTM17 had a slightly higher fluorescence intensity than mTM17 and its spectrum displayed a slight blue-shift (Table 2). As for the TM16 fragments, log-normal decomposition of the fluorescence emission spectra showed bimodal emission. We noticed a significant blue-shift (particularly in DM) of each W10 elemental spectrum with respect to that of W20, corresponding to a location of W10 in DM micelles deeper than that of W20.

3.3. Quenching, by acrylamide, of the fluorescence of the Trp residue in the TM16 and TM17 fragments incorporated into DM and DPC micelles

We evaluated Trp insertion into detergent micelles, by assessing its accessibility to the neutral water-soluble fluorescent quencher acrylamide [57]. The Stern–Volmer fluorescence quenching plots obtained for the TM16 peptides in the presence of DM or DPC

Table 2
Fluorescence emission spectra decomposition into log-normal Gaussian curves for the TM16 and TM17 fragments in DPC or DM micelles. The decomposition procedure is detailed in Materials and methods. λ_{max} is calculated as $10^4/\nu_m$ and the spectrum peak height is calculated as $I_{max}/\Sigma I_{max}$. FWHM is the spectrum full width at half-maximum. The skewness parameter was kept constant at 1.042.

Peptide	Solvent	Raw spectrum	Log-normal Gaussian no. 1			Log-normal Gaussian no. 2		
		λ_{max} (nm)	λ_{max} (nm)	FWHM (cm^{-1})	Peak height (%)	λ_{max} (nm)	FWHM (cm^{-1})	Peak height (%)
mTM16	DPC	335	326	3604	38	345	4858	62
W19-mTM16	DPC	334	324	3582	34	345	4935	66
mTM16	DM	332	323	3652	39	342	5012	61
W19-mTM16	DM	331	321	3497	38	341	4989	62
mTM17	DPC	337	331	4488	51	348	5277	49
W10-mTM17	DPC	335	327	4292	37	342	6285	63
mTM17	DM	337	330	4787	44	346	5412	56
W10-mTM17	DM	330	318	3816	30	337	5251	70

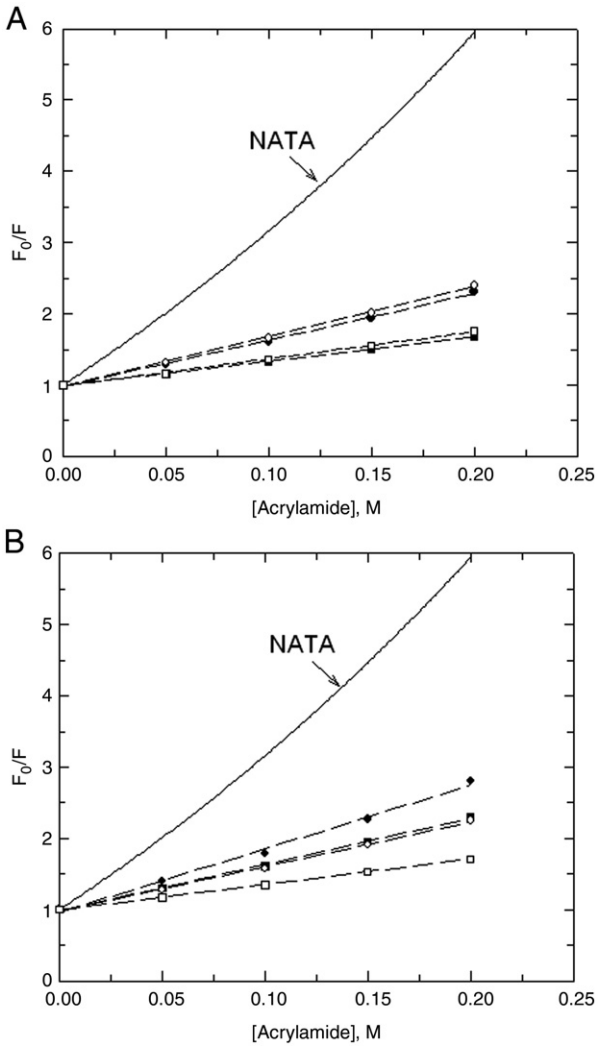

Fig. 3. Stern–Volmer plots of the quenching by acrylamide of the fluorescence of hMRP1 fragments in DPC and DM micelles. (A) We added 8 μM mTM16 (closed symbols) or 5 μM W19-mTM16 (open symbols) to 10 mM potassium phosphate buffer pH 7.5, at 20 °C, supplemented with 4 mM DPC (circles) or DM (squares). Aliquots of acrylamide were then added sequentially, at constant intervals (100 s). Fluorescence intensity was continuously recorded with λ_{ex} set at 295 nm and λ_{em} set at 340 nm. Slit widths were 1.25 mm for excitation and 2.5 mm for emission. The fluorescence intensities obtained at each acrylamide concentration were corrected for blank values. The Stern–Volmer plot for NATA (5 μM) in buffer (λ_{em} = 354 nm in this case) is also shown, as a reference (continuous line). A straight line was fitted to the data for MRP1 fragments, whereas the modified Stern–Volmer equation was used for NATA. (B) Similar experiment as in panel A, but with 5 μM mTM17 (closed symbols) or W10-mTM17 (open symbols).

micelles are shown in Fig. 3A. Linear regressions were appropriate and typical of a collisional (dynamic) mechanism. Similar behavior was observed for mTM17 [37] and W10-mTM17 (Fig. 3B). The apparent accessibility to acrylamide of the Trp residues in the studied peptides incorporated into detergent micelles was significantly lower than that of NATA in buffer, taken as a reference (Fig. 3 and K_{sv} in Table 3). A more accurate comparison of solvent accessibility can be made on the basis of bimolecular quenching constants k_q than based on K_{sv}, because the differences in $\langle\tau\rangle$, the amplitude-averaged excited state lifetime of the Trp residue in the absence of quencher, are taken into account ($k_q = K_{sv}/\langle\tau\rangle$). k_q values ranged from 20% to ~50% compared to that of NATA (Table 3). In both detergents, each mutant peptide was less accessible to acrylamide than the corresponding "native" peptide. In addition, the Trp residue of each peptide was less accessible to acrylamide in DM micelles than in DPC micelles. Finally, consistent with previous findings [37], the W20 residue at the C-terminus of mTM17 was largely accessible to solvent, whereas W19 at the C-terminus of W19-mTM16 was the more shielded from acrylamide.

3.4. Quenching, by brominated detergents, of the fluorescence of the Trp residue in the TM16 and TM17 fragments incorporated into DM and DPC micelles

We investigated the location of Trp in the micelles in more detail, by carrying out Trp quenching experiments with two brominated analogs of DM: BrDM, brominated at the C7 and C8 positions of the alkyl chain, and BrUM, brominated at the C10 and C11 positions. The results obtained were compared with the calibration results obtained with a set of α-helical transmembrane model peptides [40]. Quenching occurs when bromine atoms come into contact with or are located very close to Trp. Quenching data therefore reflect the accessibility of Trp to the alkyl chains.

The Trp quenching plots for mTM16 and W19-mTM16 are shown in Fig. 4. With BrDM (panel A) or BrUM (panel B) used as the quencher, W19 was more strongly quenched than W4 (mTM16) at each concentration of brominated detergent, implying greater contact with the brominated detergent chains. In all cases, the residual fluorescence for completely brominated detergent ($X = 1$) was low, below 20%, providing direct evidence for the insertion of the peptides into micelles. The difference between the two Trp residues is described more quantitatively by the parameters of the fits, n and F_{min}/F_0, given in Table 4. Higher values of n are associated with greater accessibility of the Trp in the peptide to the brominated chain of the detergent. Clearly, W19, for which up to 96% quenching was observed, with $n = 3.8$ and 3.7, was more accessible to the brominated chains than W4.

Comparison of the Trp quenching plots for the W10-mTM17 mutant and for mTM17 (Fig. 5) clearly indicated that W10 was more accessible to the brominated chains than W20, as also shown in Table 4.

These results are consistent with those obtained with acrylamide because, for each fragment, greater Trp accessibility to bromine is associated with lower Trp accessibility to acrylamide.

For a more detailed interpretation, the insets show the position of the n values obtained here with those obtained with model peptides. The calibration curve obtained with BrUM (inset in Figs. 4 and 5, panel

Table 3
Parameters of the quenching by acrylamide of the fluorescence of various MRP1 peptides in DPC and DM micelles.

Sample	Medium	$\langle\tau\rangle$ (ns)	K_{sv} (M^{-1})	k_q (M^{-1} s^{-1}) (% of reference)
NATA	Buffer	3.0	17.5	5.83×10^9 (100%)
mTM16	DPC micelles	2.97	6.54	2.20×10^9 (38%)
W19-mTM16	DPC micelles	4.37	6.98	1.60×10^9 (27%)
mTM16	DM micelles	2.54	3.40	1.34×10^9 (23%)
W19-mTM16	DM micelles	3.29	3.82	1.16×10^9 (20%)
mTM17	DPC micelles	2.92	8.94	3.06×10^9 (52%)
W10-mTM17	DPC micelles	2.87	6.26	2.18×10^9 (37%)
mTM17	DM micelles	2.45	6.5	2.65×10^9 (45%)
W10-mTM17	DM micelles	2.44	3.56	1.45×10^9 (25%)

For peptides, the amplitude-averaged lifetime values, $\langle\tau\rangle = \Sigma\alpha_i\tau_i$, were taken from Table 5. For NATA, $\langle\tau\rangle$ was taken from a previous study [119]. K_{sv} is the slope from Fig. 3. $k_q = K_{sv}/\langle\tau\rangle$.

B) is more regular than that obtained with BrDM, due to the bromine being located at the end of the detergent chain. Trp fluorescence in the various MRP1 fragments was quenched to various extents by BrUM, but none of the *n* values obtained reached those obtained for the P9, P11 and P13 model peptides, for which Trp is located in the inner core of the micelle. The location of the Trp residues of TM16 and TM17 may therefore be restricted to the polar head group region of the micelle.

3.5. Time-resolved fluorescence intensity measurements for the Trp residues in the TM16 and TM17 fragments incorporated into DM and DPC micelles

The fluorescence intensity decays of the Trp residues in all the studied peptides, whether in buffer solution or incorporated into detergent micelles, were multiexponential (Fig. 6A). Three excited state lifetime populations resulted from MEM analysis in most cases (Table 5). The respective barycenter of each population for the different peptides was in the range of 0.3 to 0.75 ns for the shortest lifetime, 1.3 to 2.5 ns for the intermediate lifetime and 3.4 to 6.1 ns for the longest lifetime (Table 5). The amplitude-averaged lifetime $\langle\tau\rangle$ for W19-mTM16 was significantly higher than that for mTM16 in both detergents, consistent with the observed increase in fluorescence intensity. This effect results principally from the increase in the longest lifetime value and its amplitude. By contrast, in both mTM17 fragments, $\langle\tau\rangle$ remains approximately constant, due to compensation between a

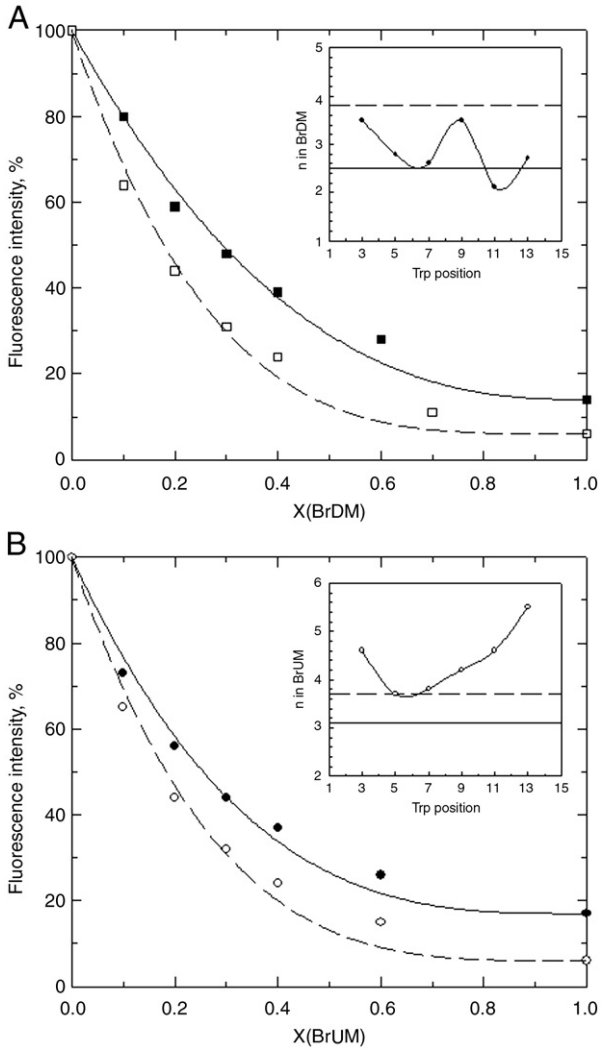

Fig. 4. Quenching of the fluorescence of hMRP1 TM16 fragments in mixed micelles of BrDM/DM (panel A) or BrUM/DM (panel B). (A) duplicate independent measurements of the fluorescence intensity (after 3 minutes of equilibration) of 5 μM mTM16 (closed symbols) or W19-mTM16 (open symbols) were made in 10 mM phosphate buffer pH 7.5, supplemented with various mixtures of BrDM and DM, at a final total detergent concentration of 4 mM, at 20 °C. Fluorescence intensity is plotted as a function of *X*, the molar fraction of brominated detergent. λ_{ex} was set at 280 nm and λ_{em} at 332 and 331 nm for mTM16 and W19-mTM16, respectively (slit width = 1.25 mm for both excitation and emission). A curve was fitted to the data, as described in Materials and methods. The insets show the calibration curves of the n parameter with Trp position, obtained with six model peptides in BrDM/DM [40]. The horizontal lines represent the n values obtained here for the TM16 fragments. (B) Similar experiment as in panel A, but with BrUM as the brominated detergent.

Table 4
Parameters of the fluorescence quenching curves of various MRP1 fragments in mixed micelles of DM with BrDM or BrUM.

Fragment	Mixed micelles	*n*	F_{min}/F_0
mTM16	DM/BrDM	2.5	14%
W19-mTM16	DM/BrDM	3.8	6%
mTM16	DM/BrUM	3.1	17%
W19-mTM16	DM/BrUM	3.7	6%
mTM17[a]	DM/BrDM	2	22%
W10-mTM17	DM/BrDM	3.7	4%
mTM17[a]	DM/BrUM	2.9	27%
W10-mTM17	DM/BrUM	4.0	5%

n and F_{min}/F_0 were obtained from the fit of the quenching curves in Fig. 4.
[a] From [37].

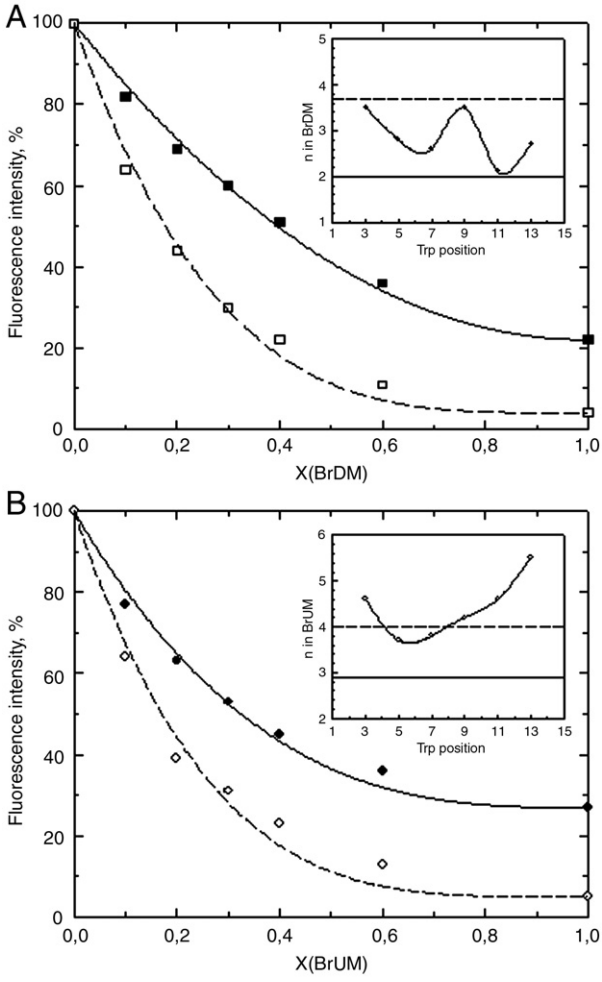

Fig. 5. Quenching of the fluorescence of hMRP1 TM17 fragments in mixed micelles of BrDM/DM (panel A) or BrUM/DM (panel B). Quenching curves for mTM17 (closed symbols) and W10-mTM17 (open symbols) with BrDM (panel A) or BrUM (panel B) as the brominated detergent. λ_{em} was set at 330 nm for W10-mTM17. The curves for mTM17 were obtained in a previous study [37] (with λ_{em} = 335 nm), and only the points at *X* = 1 were checked here. Otherwise, the experiments were performed as in Fig. 4.

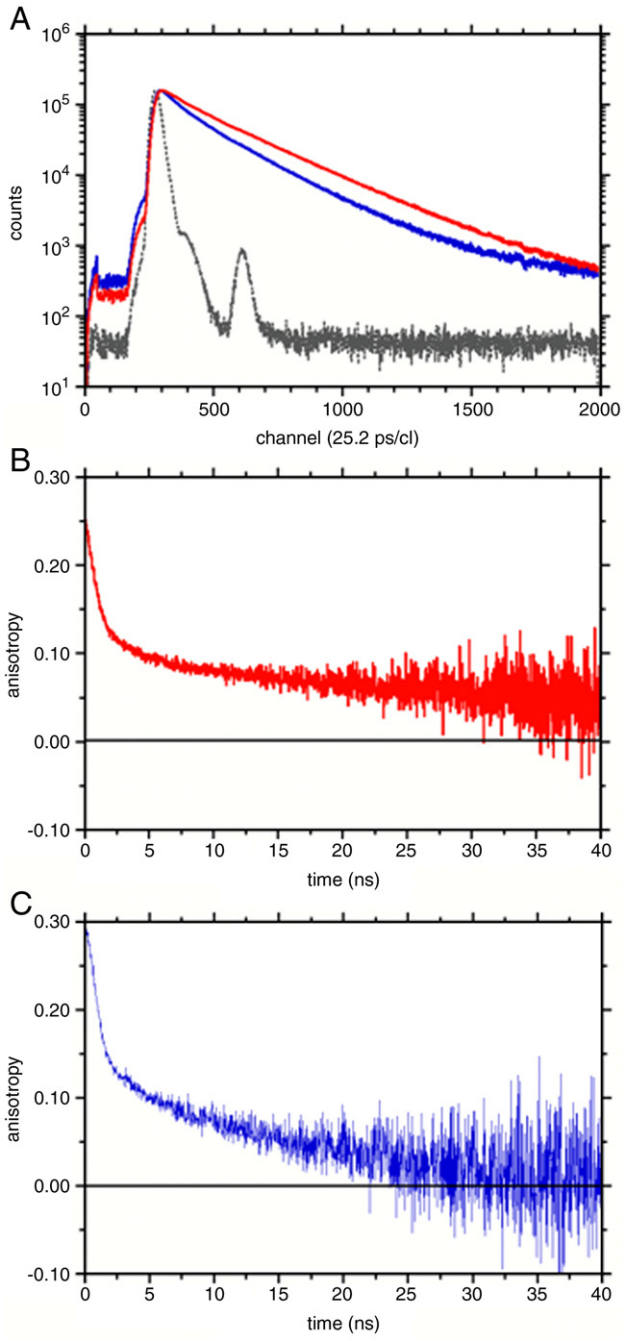

Fig. 6. Time-resolved fluorescence of hMRP1 TM16 fragments in DPC micelles. (A) Experimental fluorescence intensity decay of mTM16 (blue trace) and W19-mTM16 (red trace) in DPC. Instrumental response function (black trace). (B) Experimental fluorescence anisotropy decay of mTM16 in DPC. (C) Experimental fluorescence anisotropy decay of W19-mTM16 in DPC. Experimental conditions are described in Materials and methods. Peptide concentration: 10 μM.

small increase in the long lifetime value, a decrease in amplitude and an increase in the contribution of the intermediate lifetime (Table 5).

3.6. Dynamics of the Trp residue in the TM16 and TM17 fragments incorporated into DM and DPC micelles

Trp dynamics, which may also reflect peptide and peptide–detergent dynamics, was monitored by evaluating time-resolved fluorescence anisotropy. The experimental anisotropy decay curves of the Trp residues of these peptides in buffer and incorporated into detergent micelles included a fast component, consistent with the rapid dynamics of the indole fluorophore, followed by a slower component (Figs. 6B and C). Data analysis by MEM showed there to be two to three time components: one or two short components with values of 0.3 to 0.9 and 1.1 to 6 ns and a much longer component, with values from 12 up to 70 ns (Table 6). The shortest rotational correlation time probably reflects the local motion of the chromophore around the Cα–Cβ–Cγ bonds, whereas the intermediate time constants probably describe local peptide flexibility. The longest rotational correlation times describe the overall Brownian motion of the entire peptide–detergent assembly and peptide aggregate in buffer. Some are at the limit of what can be accurately measured, not longer than ~10 times the Trp lifetime value, i.e. ~25 to 45 ns in our experimental conditions. The rotational correlation times obtained in the presence of detergent are significantly higher than those expected for pure detergent micelles, consistent with larger aggregation numbers and/or more elongated shapes for some of the peptide–detergent assemblies. However, shorter correlation times (as seen from β_1 and β_2 values) also make a significant contribution, indicating large amplitude of motion for the Trp residues in all peptides, with wobbling-in-cone angle values in the range of 30°–38° (Table 6).

3.7. Secondary structure

We carried out a far-UV CD study of mTM16 in various conditions (Fig. 7A). The CD spectrum of mTM16 in TFE, used as a reference, is indicative of a predominantly α-helical conformation, with a characteristic high maximum at ~192 nm and two minima at ~208 and 220 nm. By contrast, the CD spectrum of mTM16 solubilized in buffer was very flat, indicating an absence of helical structure. In the presence of DM or DPC micelles, significant structural changes occurred, making it impossible to identify a predominant structure. Deconvolution of these spectra was required to identify the various spectral components.

The fractions of α-helix, β-strands, turns and unordered structures obtained for mTM16 are presented as histograms in Fig. 7B. In TFE, this fragment was mostly α-helical (~60% α-helix), as expected from the shape of its CD spectrum. In buffer alone, the structure of this fragment consisted principally of β-strands, together with unordered structures. In both DM and DPC, mTM16 appeared to be structured partly into a helix (up to 20% helical structure, potentially corresponding to a short helix consisting of five of the 25 amino acids) coexisting with significant β-strands.

The secondary structure of mTM17 has previously been analyzed by the same method in methanol, buffer, and in the presence of DM and DPC micelles [37]. This fragment had a higher tendency to be structured, with close to 80% α-helix in methanol, and up to ~50% α-helix in DPC, the most structuring detergent.

As for the variants, it is known for long that each amino acid has a certain propensity to form an α helix in a protein (or peptide). In particular, there is a correspondence between the side chain hydrophobic surface and the helix propensity, and as a consequence, Trp, Phe, and Tyr have very similar helix propensity values (0.58, 0.59, and 0.72, respectively, on a scale where the propensity is 0.00 for Gly and 0.96 for Ala) [66]. Because our mutations were only W→Y, Y→W, or F→W, we believe that only slight structural changes might have occurred.

4. Discussion

In the consensus hMRP1 topology (Scheme 1), the protein consists of three membrane-spanning domains, encompassing up to 17 putative transmembrane helices (TM) and two nucleotide-binding domains [5]. Except for MSD0, the protein is similar to other ABC transporters, "full transporters" or homodimers of "half-transporters." The recent homology modeling based on the structure of the Sav1866

Table 5
Parameters of the fluorescence intensity decays of the Trp residue in the peptides studied, in various media.

Peptide	Medium	α_1	α_2	α_3	τ_1 (ns)	τ_2 (ns)	τ_3 (ns)	$<\tau>$ (ns)[a]
mTM16	Buffer	0.40 ± 0.01	0.40 ± 0.01	0.20 ± 0.01	0.41 ± 0.08	1.51 ± 0.09	4.03 ± 0.06	1.60 ± 0.07
W19-mTM16	Buffer	0.34 ± 0.03	0.40 ± 0.03	0.26 ± 0.02	0.43 ± 0.07	1.53 ± 0.17	4.22 ± 0.37	1.87 ± 0.11
mTM16	DPC	0.27 ± 0.04	0.28 ± 0.04	0.45 ± 0.06	0.48 ± 0.18	1.93 ± 0.52	5.12 ± 0.40	2.97 ± 0.23
W19-mTM16	DPC	0.15 ± 0.07	0.18 ± 0.01	0.67 ± 0.06	0.30 ± 0.06	1.49 ± 0.42	6.05 ± 0.18	4.37 ± 0.20
mTM16	DM	0.33 ± 0.03	0.33 ± 0.03	0.34 ± 0.09	0.48 ± 0.22	2.10 ± 0.69	4.98 ± 0.67	2.54 ± 0.22
W19-mTM16	DM	0.27 ± 0.05	0.35 ± 0.06	0.38 ± 0.14	0.74 ± 0.32	2.52 ± 0.95	5.76 ± 0.85	3.29 ± 0.14
mTM17	Buffer	0.37 ± 0.11	0.38 ± 0.05	0.25 ± 0.06	0.45 ± 0.01	1.35 ± 0.29	3.42 ± 0.08	1.59 ± 0.04
W10-mTM17	Buffer	0.48 ± 0.07	0.35 ± 0.05	0.17 ± 0.02	0.40 ± 0.04	1.26 ± 0.12	3.62 ± 0.34	1.38 ± 0.25
mTM17	DPC	0.33 ± 0.02	0.22 ± 0.01	0.44 ± 0.02	0.41 ± 0.07	1.69 ± 0.41	5.24 ± 0.23	2.92 ± 0.07
W10-mTM17	DPC	0.29 ± 0.01	0.37 ± 0.04	0.34 ± 0.04	0.54 ± 0.06	2.24 ± 0.32	5.66 ± 0.29	2.87 ± 0.10
mTM17	DM	0.35 ± 0.05	0.31 ± 0.04	0.34 ± 0.03	0.33 ± 0.04	1.73 ± 0.08	5.13 ± 0.13	2.45 ± 0.23
W10-mTM17	DM	0.34 ± 0.01	0.44 ± 0.01	0.22 ± 0.02	0.55 ± 0.03	2.33 ± 0.11	5.45 ± 0.12	2.44 ± 0.04

Experimental conditions as in Fig. 6. Mean values ± standard errors on a significant number of measurements (≥2) are given.
[a] $<\tau>$ is calculated as $<\tau> = \Sigma\alpha_i\tau_i$.

transporter [24] yielded a 3D representation of the arrangement of hMRP1 TM helices in this shared membrane core [27], now suggesting the involvement of nearly all MSD1 and MSD2 TM fragments for constituting the transport pore. However, because of the low sequence similarity of hMRP1 and Sav 1866, experimental structural studies are still required.

We therefore initiated a study of the folding and topological properties of isolated TM segments from hMRP1. TM16 and TM17 [37] were first chosen for study, on the basis of previous mutational and labeling studies highlighting their importance for substrate recognition and transport by hMRP1. Each of these TM peptides contains a single-Trp residue involved in hMRP1 function. We were therefore able to make use of the high sensitivity of the fluorescence emission of tryptophan residues to their environment, making it possible to use tryptophan as a natural tag for probing environmental changes. Tryptophan fluorescence emission spectra are known to be highly sensitive to the polarity properties of the environment surrounding the tryptophan residue [67,68], with peak emission ranging from ~305 nm for total shielding from the solvent in azurin [69,70], to ~350 nm for full exposure to the solvent in small water-soluble peptides [71–73] or unfolded proteins [59,74]. Moreover, tryptophan fluorescence intensity decay is a sensitive indicator of rotamer conformation [75–80] and of interaction with the environment, such as solvent–exciplex formation [81–84] or dipolar relaxation [85–90]. We therefore used a strategy combining conservative site-specific single-Trp mutagenesis with fluorescence spectroscopy and circular dichroism spectroscopy to study the location and dynamics of these isolated TM peptides in membrane mimics constituted by detergent micelles. Based on our previous studies [37,40,48], DM and DPC were selected as suitable detergents.

Before characterizing the peptide–micelle complexes, we checked that the peptides bound to DM and DPC micelles in the usual experimental conditions for fluorescence and CD studies (μM range for peptide concentration). Peptide binding was always complete at a detergent concentration of 4 mM, as clearly exemplified for W19-mTM16. Further evidence for peptide–detergent interaction was provided by the high level of quenching of Trp fluorescence by 4 mM brominated analogs of DM (BrDM and BrUM). Quenching levels reached ~75% [37] to 95% (Figs. 4 and 5, Table 4), indicating Trp–bromine atom contact or very close proximity.

Peptide binding was expected, given the hydrophobic character of both TM16 and TM17, as quantified by their interfacial partitioning free energy for unfolded peptide (ΔG_u), which depends solely on amino acid composition [91]. With a ΔG_u of −4.1 and −6.2 kcal/mol (Table 1), native TM16 and, to a lesser extent TM17, are, however, less hydrophobic than many of the other predicted TM segments of hMRP1 and, for example, than TM1 and TM2 ($\Delta G_u = -14.7$ and −9.2 kcal/mol, respectively). The small sequence changes introduced (C → S, Trp mutation) also rendered our synthetic peptides slightly less hydrophobic than their native counterparts (Table 1).

We next characterized the emission spectra of the peptide–detergent complexes. Our previously studied transmembrane model peptides, which had single–Trp residues in various positions in the polypeptide sequence, had fluorescence emission maxima from 327–330 nm to 313–314 nm for interfacial and the deeply embedded Trp, respectively, in DM or in DPC micelles [37,40,52]. For tryptophan octyl ester, the fluorescent moiety of which is probably located close to the polar head group region, emission peaked at 335 nm in both DM and DPC micelles [52,56]. For the various TM16 fragments, incorporated into DPC or in DM, W4 and W19 mutant displayed mean maximum

Table 6
Parameters of the fluorescence anisotropy decays of the Trp residue in the peptides studied, in various media.

Peptide	Medium	β_1	β_2	β_3	θ_1 (ns)	θ_2 (ns)	θ_3 (ns)	ω_{max} (°)	$A_{t=0}$
mTM16	Buffer	–	0.027 ± 0.008	0.122 ± 0.012	–	3 ± 1	∞		0.149 ± 0.004
W19-mTM16	Buffer	–	0.032 ± 0.003	0.091 ± 0.011	–	2.3 ± 0.9	∞		0.123 ± 0.011
mTM16	DPC	–	0.040 ± 0.009	0.117 ± 0.013	–	2.7 ± 0.7	20 ± 2	31	0.157 ± 0.010
W19-mTM16	DPC	0.063 ± 0.043	0.060 ± 0.014	0.081 ± 0.014	0.3 ± 0.1	2.7 ± 0.7	49 ± 5	35	0.204 ± 0.050
mTM16	DM	–	0.033 ± 0.011	0.132 ± 0.010	–	3.1 ± 1.4	51 ± 16	30	0.165 ± 0.014
W19-mTM16	DM	0.021 ± 0.004	0.035 ± 0.008	0.091 ± 0.006	0.9 ± 0.4	3.4 ± 0.6	70 ± 19	38	0.147 ± 0.007
mTM17	Buffer	–	0.063 ± 0.003	0.063 ± 0.006	–	1.1 ± 0.1	∞		0.126 ± 0.005
W10-mTM17	Buffer	–	0.009 ± 0.007	0.104 ± 0.001	–	1.2 ± 0.6	∞		0.113 ± 0.007
mTM17	DPC	0.051 ± 0.010	0.073 ± 0.015	0.065 ± 0.012	0.30 ± 0.01	3.8 ± 0.5	17 ± 4	35	0.189 ± 0.007
W10- mTM17	DPC	0.021 ± 0.008	0.054 ± 0.030	0.083 ± 0.036	0.7 ± 0.05	3.0 ± 1.6	12 ± 3	35	0.158 ± 0.005
mTM17	DM	0.026 ± 0.004	0.061 ± 0.019	0.081 ± 0.020	0.55 ± 0.17	6.1 ± 1.0	50 ± 27	34	0.168 ± 0.004
W10-mTM17	DM	–	0.023 ± 0.008	0.115 ± 0.010	–	2.2 ± 0.5	21 ± 9	35	0.137 ± 0.010

The anisotropy β_i is the area and the rotational correlation time θ_i is the bary center of peak i of the rotational correlation time distribution. $A_{t=0}$ is the anisotropy at time zero, with $A_{t=0} = \Sigma\beta_i$. The semiangle ω_{max} of the wobbling-in-cone subnanosecond motion was calculated from: $\Sigma\beta_{ns}/A_0 = [1/2\cos\omega_{max}(1+\cos\omega_{max})]^2$, which gives: $\omega_{max} = \arccos 1/2[(1+8(\Sigma\beta_{ns}/A_0)^{1/2})^{1/2} - 1]$, where A_0 is Trp anisotropy in the absence of depolarization and β_{ns} is the anisotropies of the nanosecond components. A value of 0.251 for excitation with the picoseconds diode laser PLS295 was calculated from the wavelength convolution of the nanoLED optical power emission with the intrinsic anisotropy of NATA [37]. Mean values ± standard errors on a significant number of measurements (≥2) are given.

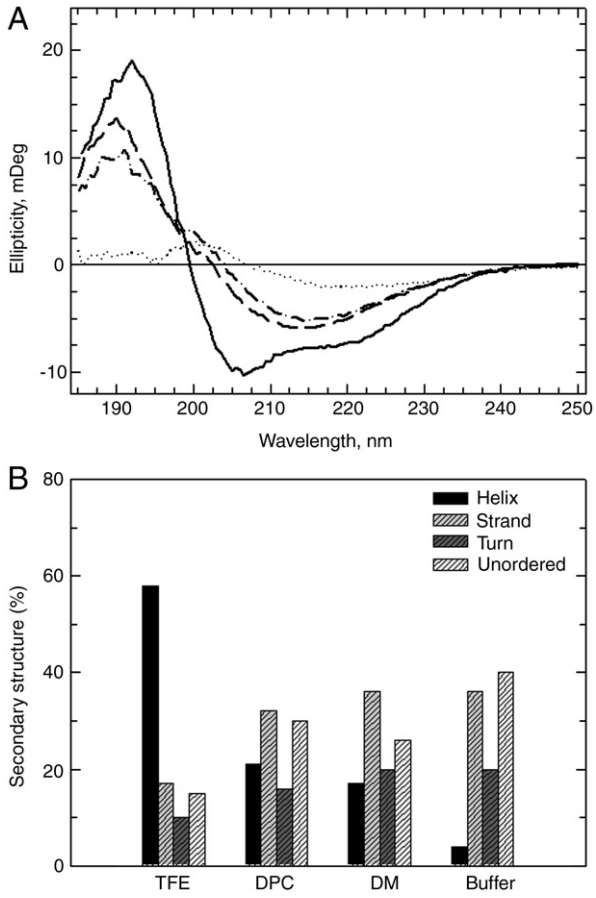

Fig. 7. Far UV CD results for mTM16 in various media. (A) CD spectra in millidegrees, for 20 μM mTM16 in a cuvette with a 1-mm path length. The medium was TFE (continuous line), buffer alone (dotted line), or contained 4 mM DPC (long-dashed line) or DM (dashed-dotted line). (B) Histograms for the various structural elements.

fluorescence emission wavelengths close to that of TOE [52,56], and slightly longer than those displayed by the Trp residue of the transmembrane model peptides (P3, P5, and P7), that were closer to the water/micelle interface in the same detergents [37,40]. The W4 or W19 residue was therefore located in the polar head group region of the detergent micelles rather than in their hydrophobic core. However, this location may be considered an average location because, as observed for the transmembrane model peptides, fluorescence emission spectra were polymodal and could be described as the sum of two elemental spectra: one with a maximum at ~321–326 nm and the other with a maximum at ~341–345 nm [37,40]. Despite small λ_{max} differences, the fluorescence emission spectra of W20 in mTM17 and W10 in W10-mTM17 were also consistent with a similar location.

According to Burstein's classification of Trp in proteins [92,93], a fluorescence emission maximum at ~325 nm corresponds to a Trp residue capable of hydrogen bonding to a water molecule (or another partner), whereas a fluorescence emission maximum at ~340 nm corresponds to a Trp residue exposed to a slowly relaxing polar solvent. Fluorescence spectrum decomposition therefore suggests that the Trp residue may fluctuate between a shallow location within micelles in which a few water molecules may hydrogen bond to the indole ring (probably the inner interface between the acyl chain and the polar head groups) and a location at the surface, where slowly relaxing water molecules are present (probably the interface between water and the polar head groups). Similar features were observed for the W19 residue of the W19-mTM16 mutant, with the exception of a slight shift in the fluorescence emission spectrum towards shorter wavelengths, indicating a slightly deeper insertion. Similarly, W10 in the mutated mTM17 peptide seemed to be located deeper in the micelle than the W20 residue in mTM17.

The differences in Trp location were investigated further, with water-soluble (acrylamide) and lipophilic (brominated analogs of DM) quenchers. The various Trp residues were all significantly shielded from acrylamide, by at least 50%, whereas all were quenched by brominated detergents to levels of up to 96%. As previously reported [37], the sum of the fluorescence intensities quenched by acrylamide in the presence of DM and by a brominated detergent (BrDM or BrUM) may exceed 100%, indicating that both bromines of the acyl chains and acrylamide may be present in the micelle region in which Trp is located. Consistent results were obtained for all the parameters related to Trp location: λ_{max} values, k_q for acrylamide accessibility, n and F_{min}/F_0 for brominated detergent accessibility. These results suggest that the peptides are inserted into the polar head group region of the micelles (DPC and DM) in an oblique orientation, as the Trp residues of the mutated peptides were embedded slightly deeper in the micelles than the corresponding native Trp residues (lower λ_{max} and lower k_q for DM and DPC and lower F_{min}/F_0 and higher n in the case of DM micelles). The more surface-exposed regions of TM16 and TM17, respectively, probed by the native Trp W4 and W20 residues, respectively (i.e., W1198 and W1246 if numbered as in hMRP1), correspond to the cytoplasmic side of the plasma membrane. Our results suggest that W1246 is the most exposed Trp residue, whereas the non-native W19 (corresponding to F1213 in the whole protein) is located deeper in the micelle. One can argue that Trp mutations may introduce artefacts in peptide position because Trp shows a preference for membrane interfaces [94]. Our variants were chosen to minimize this effect. For TM17, the Trp variant results from the two point mutations: Y1236W and W1246Y, so that the overall effect on ΔG_u (interfacial partitioning free energy of the peptide) is null. Moreover, since W and Y have a very similar distribution pattern in membranes [95], our results can be considered as quite reliable. For TM16, the variant results from the following two point mutations: W1198Y and F1113W. The variation in overall ΔG_u is not null but small (0.19 kcal/mol, as can be seen from Table 1). In this case, since F is found equally distributed throughout the transmembrane region [95], there is a slight change in the distribution tendency. However, a single W may not be sufficient to strongly modify peptide position: in this regard, in the study of Trp anchored model peptides, two consecutive Trp are put at a model peptide end to study this property (e.g., Killian et al. [96,97]). Time-resolved fluorescence analyses were carried out to gain more insight into the local conformation and dynamics of the peptide regions labeled by W4 and W19 (i.e., W1198 and W1213, respectively). In this study, MEM analysis showed that the fluorescence intensity decays of the Trp residues in the various peptides were mostly accounted for by three excited-state lifetime populations in the nanosecond time range. These lifetime values were in the same range as those characterizing the Cα–Cβ bond Trp χ_1 rotamers measured in conformationally constrained peptides [98,99]. The data were interpreted in the framework of the rotamer model [75,76], in which the lifetimes of Trp Cα–Cβ rotamers depend on their sensitivity to peptide bond quenching by electron (or proton) transfer mechanisms as a function of their geometry and environment [77,79,100–104]. The relative proportions of the rotamers were assumed to be governed by the structural constraints imposed by the main peptide chain [105,106]. Using TFE as a helix promoter, we showed that the amplitude of the longest lifetime component in single-Trp-containing peptides in solution was clearly correlated with α-helix formation [107]. The constraints imposed by the membrane or micellar environments may also affect the rotamer distribution, as suggested in our previous studies of TM model peptides in DM and DPC micelles [37,40]. Based on these considerations, the major rotamer associated with the longest lifetime observed for W19 may indicate that the C-terminal amino acids of the mTM16 peptide are folded as a helix. According to

our CD experiments, the mTM16 peptide may intrinsically fold principally as an α-helix in organic solvents such as TFE (~60%), but it folds principally as a β-strand in the presence of detergent micelles, with only a small proportion of α-helix. Its α-helix propensity is lower than that previously observed for mTM17. mTM16 does not behave as a spontaneous stable α-helical segment in membrane mimics, as would be expected for a classical transmembrane fragment. It may form a hairpin structure at the surface of the micelles or may self-associate on the micelle, despite the presence of an excess of detergent micelles over peptide (concentration). The self-association of mTM16 may be driven in part by ionic interactions. The N-terminus of mTM16 bears both positive (R) and negative (E) charges, potentially leading to a head-to-tail arrangement for the isolated peptide. Self-association would be consistent with the rotational correlation time values, which were longer than expected for detergent–peptide complexes. The presence of an interfacial peptide may also change the aggregation number of the micelle.

If these fragments do not spontaneously form transmembrane segments, this insertion may be driven by TM-TM interactions. Searches of the TM16 and TM17 sequences for known membrane helix–helix dimerization motifs, such as GxxxG [108,109], motifs including polar residues (QxxS, SxxSSxxT, serine zipper [110]) or others (e.g., leucine zipper [111] (and for review, see [112,113]; and [114], and references therein), showed no such sequences to be present, with the exception of the AxxxA (A-ALF-A) motif at the C-terminus of TM16. No corresponding sequence was found at the N-terminus of TM17, but such a sequence was identified at the N-terminus of TM15 (A-TPI-A). The two N-termini may face the C-terminus of TM16 in the membrane part of hMRP1. A recognized stabilization motif involving aromatic residues, aromatic-xx-aromatic (aromatic = W or Y) [115], is present in the C-terminus of TM17 (Y-LN-W) and may interact with a corresponding sequence when the transport pore is closed on the cytoplasmic face and open towards the extracellular space. In the opposite conformation (pore open towards the cytoplasm), the aromatic residues may interact with polar and/or cyclic substrates. TM helix–helix association may also be driven by interactions involving only two residues, via aromatic or cation–π interactions [116]. Such TM–TM associations may increase the helical content of each peptide [114], making it higher enough for the formation of a transmembrane helix.

5. Conclusion

We provide here a detailed characterization of the interaction of hMRP1 TM16 with membrane mimics and extended our previous work on TM17 [37]. We used Trp as an intrinsic fluorescent probe. For each TM, we used the single-Trp residue present in the wild-type peptide (W1198 in TM16 and W1246 in TM17) and a Trp variant (W replacing F1213 and Y1236, respectively). Both TM16 and TM17 are involved in substrate recognition and transport by hMRP1 [38,39,41,42], and these two fragments are among the least hydrophobic of the predicted TM fragments of this transporter. On the basis of spectral and Trp fluorescence quenching parameters, two loci separated by 15 and 10 amino acid residues in TM16 (W4–W19) and TM17 (W10–W20), respectively, were shown to be located in the hydrophilic region of the micelle, in slightly different microenvironments. At this interface, TM16 folds principally into β-sheets, whereas TM17 is more helical [37]. hMRP1 is known to transport polar substrates, whereas PgP/ABCB1 specifically transports hydrophobic substrates. Consistent with this finding, the topological polar surface area of various molecules was recently shown to be correlated with the probability of transport by hMRP1 [117]. The experimentally demonstrated amphipathic character of both fragments in membrane models is consistent with the creation by these fragments of a hydrophilic environment in the membrane, at least on the cytosolic leaflet. However, the final TM16 and TM17 structures within hMRP1 are likely to differ from that observed here and are probably modulated by TM–TM interactions. Further studies of these interactions are therefore one of the avenues to be explored in future analyses of the structure of this protein.

References

[1] I.B. Holland, M.A. Blight, ABC–ATPases, adaptable energy generators fuelling transmembrane movement of a variety of molecules in organisms from bacteria to humans, J. Mol. Biol. 293 (1999) 381–399.
[2] I.B. Holland, S.P.C. Cole, K. Kuchler, C.F. Higgins, ABC Proteins: From Bacteria to Man, Academic Press, 2003.
[3] M. Dean, R. Allikmets, Complete characterization of the human ABC gene family, J. Bioenerg. Biomembr. 33 (2001) 475–479.
[4] S.P. Cole, G. Bhardwaj, J.H. Gerlach, J.E. Mackie, C.E. Grant, K.C. Almquist, A.J. Stewart, E.U. Kurz, A.M. Duncan, R.G. Deeley, Overexpression of a transporter gene in a multidrug-resistant human lung cancer cell line, Science 258 (1992) 1650–1654.
[5] R.G. Deeley, S.P. Cole, Substrate recognition and transport by multidrug resistance protein 1 (ABCC1), FEBS Lett. 580 (2006) 1103–1111.
[6] R.G. Deeley, C. Westlake, S.P. Cole, Transmembrane transport of endo- and xenobiotics by mammalian ATP-binding cassette multidrug resistance proteins, Physiol. Rev. 86 (2006) 849–899.
[7] S.P. Cole, R.G. Deeley, Transport of glutathione and glutathione conjugates by MRP1, Trends Pharmacol. Sci. 27 (2006) 438–446.
[8] D.W. Loe, K.C. Almquist, R.G. Deeley, S.P. Cole, Multidrug resistance protein (MRP)-mediated transport of leukotriene C4 and chemotherapeutic agents in membrane vesicles. Demonstration of glutathione-dependent vincristine transport, J. Biol. Chem. 271 (1996) 9675–9682.
[9] G. Rappa, A. Lorico, R.A. Flavell, A.C. Sartorelli, Evidence that the multidrug resistance protein (MRP) functions as a co-transporter of glutathione and natural product toxins, Cancer Res. 57 (1997) 5232–5237.
[10] P. Borst, N. Zelcer, K. van de Wetering, B. Poolman, On the putative co-transport of drugs by multidrug resistance proteins, FEBS Lett. 580 (2006) 1085–1093.
[11] A. Rothnie, G. Conseil, A.Y. Lau, R.G. Deeley, S.P. Cole, Mechanistic differences between GSH transport by multidrug resistance protein 1 (MRP1/ABCC1) and GSH modulation of MRP1-mediated transport, Mol. Pharmacol. 74 (2008) 1630–1640.
[12] C.E. Grant, M. Gao, M.K. DeGorter, S.P. Cole, R.G. Deeley, Structural determinants of substrate specificity differences between human multidrug resistance protein (MRP) 1 (ABCC1) and MRP3 (ABCC3), Drug Metab. Dispos. 36 (2008) 2571–2581.
[13] S.V. Ambudkar, C. Kimchi-Sarfaty, Z.E. Sauna, M.M. Gottesman, P-glycoprotein: from genomics to mechanism, Oncogene 22 (2003) 7468–7485.
[14] R.W. Robey, K.K. To, O. Polgar, M. Dohse, P. Fetsch, M. Dean, S.E. Bates, ABCG2: a perspective, Adv. Drug Deliv. Rev. 61 (2009) 3–13.
[15] A. Haimeur, G. Conseil, R.G. Deeley, S.P. Cole, The MRP-related and BCRP/ABCG2 multidrug resistance proteins: biology, substrate specificity and regulation, Curr. Drug Metab. 5 (2004) 21–53.
[16] E.M. Leslie, R.G. Deeley, S.P. Cole, Multidrug resistance proteins: role of P-glycoprotein, MRP1, MRP2, and BCRP (ABCG2) in tissue defense, Toxicol. Appl. Pharmacol. 204 (2005) 216–237.
[17] F.J. Sharom, ABC multidrug transporters: structure, function and role in chemoresistance, Pharmacogenomics 9 (2008) 105–127.
[18] C. Kast, P. Gros, Topology mapping of the amino-terminal half of multidrug resistance-associated protein by epitope insertion and immunofluorescence, J. Biol. Chem. 272 (1997) 26479–26487.
[19] C. Kast, P. Gros, Epitope insertion favors a six transmembrane domain model for the carboxy-terminal portion of the multidrug resistance-associated protein, Biochemistry 37 (1998) 2305–2313.
[20] D.R. Hipfner, K.C. Almquist, E.M. Leslie, J.H. Gerlach, C.E. Grant, R.G. Deeley, S.P. Cole, Membrane topology of the multidrug resistance protein (MRP). A study of glycosylation-site mutants reveals an extracytosolic NH2 terminus, J. Biol. Chem. 272 (1997) 23623–23630.
[21] G.E. Tusnady, B. Sarkadi, I. Simon, A. Varadi, Membrane topology of human ABC proteins, FEBS Lett. 580 (2006) 1017–1022.
[22] K. Hollenstein, R.J. Dawson, K.P. Locher, Structure and mechanism of ABC transporter proteins, Curr. Opin. Struct. Biol. 17 (2007) 412–418.
[23] G. Miller, Scientific publishing. A scientist's nightmare: software problem leads to five retractions, Science 314 (2006) 1856–1857.
[24] R.J. Dawson, K.P. Locher, Structure of a bacterial multidrug ABC transporter, Nature 443 (2006) 180–185.
[25] R.J. Dawson, K.P. Locher, Structure of the multidrug ABC transporter Sav1866 from *Staphylococcus aureus* in complex with AMP–PNP, FEBS Lett. 581 (2007) 935–938.
[26] J.D. Campbell, K. Koike, C. Moreau, M.S. Sansom, R.G. Deeley, S.P. Cole, Molecular modeling correctly predicts the functional importance of Phe594 in transmembrane helix 11 of the multidrug resistance protein, MRP1 (ABCC1), J. Biol. Chem. 279 (2004) 463–468.
[27] M.K. DeGorter, G. Conseil, R.G. Deeley, R.L. Campbell, S.P. Cole, Molecular modeling of the human multidrug resistance protein 1 (MRP1/ABCC1), Biochem. Biophys. Res. Commun. 365 (2008) 29–34.
[28] J.F. Hunt, T.N. Earnest, O. Bousche, K. Kalghatgi, K. Reilly, C. Horvath, K.J. Rothschild, D.M. Engelman, A biophysical study of integral membrane protein folding, Biochemistry 36 (1997) 15156–15176.

[29] A. Rath, D.V. Tulumello, C.M. Deber, Peptide models of membrane protein folding, Biochemistry 48 (2009) 3036–3045.
[30] J.L. Popot, D.M. Engelman, Membrane protein folding and oligomerization: the two-stage model, Biochemistry 29 (1990) 4031–4037.
[31] J.L. Popot, D.M. Engelman, Helical membrane protein folding, stability, and evolution, Annu. Rev. Biochem. 69 (2000) 881–922.
[32] M.J. Liao, E. London, H.G. Khorana, Regeneration of the native bacteriorhodopsin structure from two chymotryptic fragments, J. Biol. Chem. 258 (1983) 9949–9955.
[33] D.M. Engelman, Y. Chen, C.N. Chin, A.R. Curran, A.M. Dixon, A.D. Dupuy, A.S. Lee, U. Lehnert, E.E. Matthews, Y.K. Reshetnyak, A. Senes, J.L. Popot, Membrane protein folding: beyond the two stage model, FEBS Lett. 555 (2003) 122–125.
[34] S.H. White, W.C. Wimley, Membrane protein folding and stability: physical principles, Annu. Rev. Biophys. Biomol. Struct. 28 (1999) 319–365.
[35] C. Lundin, H. Kim, I. Nilsson, S.H. White, G. von Heijne, Molecular code for protein insertion in the endoplasmic reticulum membrane is similar for N(in)–C(out) and N(out)–C(in) transmembrane helices, Proc. Natl. Acad. Sci. U. S. A. 105 (2008) 15702–15707.
[36] A. Bernsel, H. Viklund, J. Falk, E. Lindahl, G. von Heijne, A. Elofsson, Prediction of membrane-protein topology from first principles, Proc. Natl. Acad. Sci. U. S. A. 105 (2008) 7177–7181.
[37] M. Vincent, J. Gallay, N. Jamin, M. Garrigos, B. de Foresta, The predicted transmembrane fragment 17 of the human multidrug resistance protein 1 (MRP1) behaves as an interfacial helix in membrane mimics, Biochim. Biophys. Acta 1768 (2007) 538–552.
[38] D.W. Zhang, S.P. Cole, R.G. Deeley, Determinants of the substrate specificity of multidrug resistance protein 1: role of amino acid residues with hydrogen bonding potential in predicted transmembrane helix 17, J. Biol. Chem. 277 (2002) 20934–20941.
[39] K. Ito, S.L. Olsen, W. Qiu, R.G. Deeley, S.P. Cole, Mutation of a single conserved tryptophan in multidrug resistance protein 1 (MRP1/ABCC1) results in loss of drug resistance and selective loss of organic anion transport, J. Biol. Chem. 276 (2001) 15616–15624.
[40] B. de Foresta, L. Tortech, M. Vincent, J. Gallay, Location and dynamics of tryptophan in transmembrane alpha-helix peptides: a fluorescence and circular dichroism study, Eur. Biophys. J. 31 (2002) 185–197.
[41] D. Situ, A. Haimeur, G. Conseil, K.E. Sparks, D. Zhang, R.G. Deeley, S.P. Cole, Mutational analysis of ionizable residues proximal to the cytoplasmic interface of membrane spanning domain 3 of the multidrug resistance protein, MRP1 (ABCC1): glutamate 1204 is important for both the expression and catalytic activity of the transporter, J. Biol. Chem. 279 (2004) 38871–38880.
[42] K. Koike, C.J. Oleschuk, A. Haimeur, S.L. Olsen, R.G. Deeley, S.P. Cole, Multiple membrane-associated tryptophan residues contribute to the transport activity and substrate specificity of the human multidrug resistance protein, MRP1, J. Biol. Chem. 277 (2002) 49495–49503.
[43] G. Conseil, R.G. Deeley, S.P. Cole, Functional importance of three basic residues clustered at the cytosolic interface of transmembrane helix 15 in the multidrug and organic anion transporter MRP1 (ABCC1), J. Biol. Chem. 281 (2006) 43–50.
[44] I.J. Letourneau, A. Nakajima, R.G. Deeley, S.P. Cole, Role of proline 1150 in functional interactions between the membrane spanning domains and nucleotide binding domains of the MRP1 (ABCC1) transporter, Biochem. Pharmacol. 75 (2008) 1659–1669.
[45] G. Conseil, A.J. Rothnie, R.G. Deeley, S.P. Cole, Multiple roles of charged amino acids in cytoplasmic loop 7 for expression and function of the multidrug and organic anion transporter MRP1 (ABCC1), Mol. Pharmacol. 75 (2009) 397–406.
[46] X.Q. Ren, T. Furukawa, M. Yamamoto, S. Aoki, M. Kobayashi, M. Nakagawa, S. Akiyama, A functional role of intracellular loops of human multidrug resistance protein 1, J. Biochem. 140 (2006) 313–318.
[47] E.M. Leslie, I.J. Letourneau, R.G. Deeley, S.P. Cole, Functional and structural consequences of cysteine substitutions in the NH2 proximal region of the human multidrug resistance protein 1 (MRP1/ABCC1), Biochemistry 42 (2003) 5214–5224.
[48] Y.M. Coïc, M. Vincent, J. Gallay, F. Baleux, F. Mousson, V. Beswick, J.M. Neumann, B. de Foresta, Single-spanning membrane protein insertion in membrane mimetic systems: role and localization of aromatic residues, Eur. Biophys. J. 35 (2005) 27–39.
[49] V. Beswick, R. Guerois, F. Cordier-Ochsenbein, Y.M. Coïc, T. Huynh-Dinh, J. Tostain, J.P. Noël, A. Sanson, J.M. Neumann, Dodecylphosphocholine micelles as a membrane-like environment: new results from NMR relaxation and paramagnetic relaxation enhancement analysis, Eur. Biophys. J. 28 (1998) 48–58.
[50] J. Lauterwein, C. Bösch, L.R. Brown, K. Wüthrich, Physicochemical studies of the protein-lipid interactions in melittin-containing micelles, Biochim. Biophys. Acta 556 (1979) 244–264.
[51] B. de Foresta, N. Legros, D. Plusquellec, M. le Maire, P. Champeil, Brominated detergents as tools to study protein-detergent interactions, Eur. J. Biochem. 241 (1996) 343–354.
[52] B. de Foresta, J. Gallay, J. Sopkova, P. Champeil, M. Vincent, Tryptophan octyl ester in detergent micelles of dodecylmaltoside: fluorescence properties and quenching by brominated detergent analogs, Biophys. J. 77 (1999) 3071–3084.
[53] J.V. Moller, M. le Maire, Detergent binding as a measure of hydrophobic surface area of integral membrane proteins, J. Biol. Chem. 268 (1993) 18659–18672.
[54] E.A. Burstein, S.M. Abornev, Y.K. Reshetnyak, Decomposition of protein tryptophan fluorescence spectra into log-normal components: I. Decomposition algorithms, Biophys. J. 81 (2001) 1699–1709.
[55] E.A. Burstein, V.I. Emelyanenko, Log-normal description of fluorescence spectra of organic fluorophores, Photochem. Photobiol. 64 (1996) 316–320.
[56] L. Tortech, C. Jaxel, M. Vincent, J. Gallay, B. de Foresta, The polar headgroup of the detergent governs the accessibility to water of tryptophan octyl ester in host micelles, Biochim. Biophys. Acta 1514 (2001) 76–86.
[57] M.R. Eftink, Fluorescence techniques for studying protein structure, Methods Biochem. Anal. 35 (1991) 127–205.
[58] A.K. Livesey, J.C. Brochon, Analyzing the distribution of decay constants in pulse-fluorimetry using the maximum entropy method, Biophys. J. 52 (1987) 693–706.
[59] M. Vincent, J.C. Brochon, F. Merola, W. Jordi, J. Gallay, Nanosecond dynamics of horse heart apocytochrome c in aqueous solution as studied by time-resolved fluorescence of the single tryptophan residue (Trp-59), Biochemistry 27 (1988) 8752–8761.
[60] M. Vincent, J. Gallay, The interactions of horse heart apocytochrome c with phospholipid vesicles and surfactant micelles: time-resolved fluorescence study of the single tryptophan residue (Trp-59), Eur. Biophys. J. 20 (1991) 183–191.
[61] J.C. Brochon, Maximum entropy method of data analysis in time-resolved spectroscopy, Methods Enzymol. 240 (1994) 262–311.
[62] L. Whitmore, B.A. Wallace, DICHROWEB, an online server for protein secondary structure analyses from circular dichroism spectroscopic data, Nucleic Acid Res. 32 (2004) W668–W673.
[63] L. Whitmore, B.A. Wallace, Protein secondary structure analyses from circular dichroism spectroscopy: methods and reference databases, Biopolymers 89 (2008) 392–400.
[64] D.B. Siano, D.E. Metzler, Band shapes of the electronic spectra of complex molecules, J. Chem. Phys. 51 (1969) 1856–1861.
[65] M. Vincent, B. de Foresta, J. Gallay, Nanosecond dynamics of a mimicked membrane–water interface observed by time-resolved stokes shift of LAURDAN, Biophys. J. 88 (2005) 4337–4350.
[66] M. Blaber, X.J. Zhang, B.W. Matthews, Structural basis of amino acid alpha helix propensity, Science 260 (1993) 1637–1640.
[67] D.W. Pierce, S.G. Boxer, Stark effect spectroscopy of tryptophan, Biophys. J. 68 (1995) 1583–1591.
[68] P.R. Callis, B.K. Burgess, Tryptophan fluorescence shifts in proteins from hybrid simulations: an electrostatic approach, J. Phys. Chem., B 101 (1997) 9429–9432.
[69] M.R. Eftink, C.A. Ghiron, Exposure of tryptophanyl residues in proteins. Quantitative determination by fluorescence quenching studies, Biochemistry 15 (1976) 672–680.
[70] A.G. Szabo, T.M. Stepanik, D.M. Wayner, N.M. Young, Conformational heterogeneity of the copper binding site in azurin. A time-resolved fluorescence study, Biophys. J. 41 (1983) 233–244.
[71] J. Gallay, M. Vincent, C. Nicot, M. Waks, Conformational aspects and rotational dynamics of synthetic adrenocorticotropin-(1–24) and glucagon in reverse micelles, Biochemistry 26 (1987) 5738–5747.
[72] I.M. Li De La Sierra, M. Vincent, G. Padron, J. Gallay, Interaction of recombinant human epidermal growth factor with phospholipid vesicles. A steady-state and time-resolved fluorescence study of the bis-tryptophan sequence (Trp49–Trp50), Eur. Biophys. J. 21 (1992) 337–344.
[73] A.K. Ghosh, R. Rukmini, A. Chattopadhyay, Modulation of tryptophan environment in membrane-bound melittin by negatively charged phospholipids: implications in membrane organization and function, Biochemistry 36 (1997) 14291–14305.
[74] C. Nicot, M. Vacher, M. Vincent, J. Gallay, M. Waks, Membrane proteins in reverse micelles: myelin basic protein in a membrane–mimetic environment, Biochemistry 24 (1985) 7024–7032.
[75] B. Donzel, P. Gauduchon, P. Wahl, Study of conformation in excited state of 2 tryptophanyl diketopiperazines, J. Am. Chem. Soc. 96 (1974) 801–808.
[76] A.G. Szabo, D.M. Rayner, Fluorescence decay of tryptophan conformers in aqueous-solution, J. Am. Chem. Soc. 102 (1980) 554–563.
[77] M. Hellings, M. De Maeyer, S. Verheyden, Q. Hao, E.J. Van Damme, W.J. Peumans, Y. Engelborghs, The dead-end elimination method, tryptophan rotamers, and fluorescence lifetimes, Biophys. J. 85 (2003) 1894–1902.
[78] S.L. Moors, M. Hellings, M. De Maeyer, Y. Engelborghs, A. Ceulemans, Tryptophan rotamers as evidenced by X-ray, fluorescence lifetimes, and molecular dynamics modeling, Biophys. J. 91 (2006) 816–823.
[79] P.R. Callis, A. Petrenko, P.L. Muino, J.R. Tusell, Ab initio prediction of tryptophan fluorescence quenching by protein electric field enabled electron transfer, J. Phys. Chem., B 111 (2007) 10335–10339.
[80] G. Maglia, A. Jonckheer, M. De Maeyer, J.M. Frere, Y. Engelborghs, An unusual red-edge excitation and time-dependent Stokes shift in the single tryptophan mutant protein DD-carboxypeptidase from *Streptomyces*: the role of dynamics and tryptophan rotamers, Protein Sci. 17 (2008) 352–361.
[81] M.S. Walker, T.W. Bednar, R. Lumry, Exciplex formation in the excited state of indole, J. Chem. Phys. 45 (1966) 3455–3456.
[82] T.E.F. Gudgin, W.R. Ware, The time dependence of the low-temperature fluorescence of tryptophan, J. Phys. Chem. 88 (1984) 4626–4631.
[83] K.J. Willis, A.G. Szabo, D.T. Kracjarski, Excited state reaction and the origin of the biexponential fluorescence decay of tryptophan zwitterion, Chem. Phys. Lett. 182 (1991) 614–616.
[84] N. Vekshin, M. Vincent, J. Gallay, Excited state lifetime distributions of tryptophan fluorescence in polar solutions—evidence for solvent exciplex formation, Chem. Phys. Lett. 199 (1992) 459–464.
[85] D. Toptygin, L. Brand, Spectrally- and time-resolved fluorescence emission of indole during solvent relaxation: a quantitative model, Chem. Phys. Lett. 322 (2000) 496–502.

[86] J.R. Lakowicz, On spectral relaxation in proteins, Photochem. Photobiol. 72 (2000) 421–437.
[87] M. Vincent, A.M. Gilles, I.M. Li de la Sierra, P. Briozzo, O. Barzu, J. Gallay, Nanosecond fluorescence dynamic Stokes shift of tryptophan in a protein matrix, J. Phys. Chem., B 104 (2000) 11286–11295.
[88] S.K. Pal, J. Peon, A.H. Zewail, Biological water at the protein surface: dynamical solvation probed directly with femtosecond resolution, Proc. Natl. Acad. Sci. U. S. A. 99 (2002) 1763–1768.
[89] L. Zhang, Y.T. Kao, W. Qiu, L. Wang, D. Zhong, Femtosecond studies of tryptophan fluorescence dynamics in proteins: local solvation and electronic quenching, J. Phys. Chem., B 110 (2006) 18097–18103.
[90] D. Toptygin, A.M. Gronenborn, L. Brand, Nanosecond relaxation dynamics of protein GB1 identified by the time-dependent red shift in the fluorescence of tryptophan and 5-fluorotryptophan, J. Phys. Chem., B 110 (2006) 26292–26302.
[91] K. Hristova, S.H. White, An experiment-based algorithm for predicting the partitioning of unfolded peptides into phosphatidylcholine bilayer interfaces, Biochemistry 44 (2005) 12614–12619.
[92] Y.K. Reshetnyak, Y. Koshevnik, E.A. Burstein, Decomposition of protein tryptophan fluorescence spectra into log-normal components. III. Correlation between fluorescence and microenvironment parameters of individual tryptophan residues, Biophys. J. 81 (2001) 1735–1758.
[93] Y.K. Reshetnyak, E.A. Burstein, Decomposition of protein tryptophan fluorescence spectra into log-normal components. II. The statistical proof of discreteness of tryptophan classes in proteins, Biophys. J. 81 (2001) 1710–1734.
[94] W.M. Yau, W.C. Wimley, K. Gawrisch, S.H. White, The preference of tryptophan for membrane interfaces, Biochemistry 37 (1998) 14713–14718.
[95] M.B. Ulmschneider, M.S.P. Sansom, Amino acid distributions in integral membrane protein structures, Biochim. Biophys. Acta (BBA) – Biomembr. 1512 (2001) 1–14.
[96] M.R. de Planque, E. Goormaghtigh, D.V. Greathouse, R.E.I. Koeppe, J.A. Kruijtzer, R.M. Liskamp, B. de Kruijff, J.A. Killian, Sensitivity of single membrane-spanning α-helical peptides to hydrophobic mismatch with a lipid bilayer: effects on backbone structure, orientation, and extent of membrane incorporation, Biochemistry 40 (2001) 5000–5010.
[97] M.R. de Planque, B.B. Bonev, J.A. Demmers, D.V. Greathouse, R.E. Koeppe II, F. Separovic, A. Watts, J.A. Killian, Interfacial anchor properties of tryptophan residues in transmembrane peptides can dominate over hydrophobic matching effects in peptide-lipid interactions, Biochemistry 42 (2003) 5341–5348.
[98] P.D. Adams, Y. Chen, K. Ma, M.G. Zagorski, F.D. Sönnichsen, M.L. McLaughlin, M.D. Barkley, Intramolecular quenching of tryptophan fluorescence by the peptide bond in cyclic hexapeptides, J. Am. Chem. Soc. 124 (2002) 9278–9286.
[99] C.P. Pan, M.D. Barkley, Conformational effects on tryptophan fluorescence in cyclic hexapeptides, Biophys. J. 86 (2004) 3828–3835.
[100] R.W. Cowgill, Fluorescence and protein structure. XVII. On the mechanism of peptide quenching, Biochim. Biophys. Acta 200 (1970) 18–25.
[101] J.W. Petrich, M.C. Chang, D.B. McDonald, G.R. Fleming, On the origin of non-exponential fluorescence decay in tryptophan and its derivatives, J. Am. Chem. Soc. 105 (1983) 3824–3832.
[102] Y. Chen, B. Liu, H.T. Yu, M.D. Barkley, The peptide bond quenches indole fluorescence, J. Am. Chem. Soc. 118 (1996) 9271–9278.
[103] A. Ababou, E. Bombarda, On the involvement of electron transfer reactions in the fluorescence decay kinetics heterogeneity of proteins, Protein Sci. 10 (2001) 2102–2113.
[104] P.L. Muino, P.R. Callis, Solvent effects on the fluorescence quenching of tryptophan by amides via electron transfer. Experimental and computational studies (dagger), J. Phys. Chem., B 113 (2009) 2572–2577.
[105] K.J. Willis, W. Neugebauer, M. Sikorska, A.G. Szabo, Probing α-helical secondary structure at a specific site in model peptides via restriction of tryptophan side-chain rotamer conformation, Biophys. J. 66 (1994) 1623–1630.
[106] A.H. Clayton, W.H. Sawyer, Tryptophan rotamer distributions in amphipathic peptides at a lipid surface, Biophys. J. 76 (1999) 3235–3242.
[107] A. Bouhss, M. Vincent, H. Munier, A.M. Gilles, M. Takahashi, O. Bârzu, A. Danchin, J. Gallay, Conformational transitions within the calmodulin-binding site of *Bordetella pertussis* adenylate cyclase studied by time-resolved fluorescence of Trp242 and circular dichroism, Eur. J. Biochem. 237 (1996) 619–628.
[108] M.A. Lemmon, J.M. Flanagan, H.R. Treutlein, J. Zhang, D.M. Engelman, Sequence specificity in the dimerization of transmembrane alpha-helices, Biochemistry 31 (1992) 12719–12725.
[109] M.A. Lemmon, J.M. Flanagan, J.F. Hunt, B.D. Adair, B.J. Bormann, C.E. Dempsey, D. M. Engelman, Glycophorin A dimerization is driven by specific interactions between transmembrane alpha-helices, J. Biol. Chem. 267 (1992) 7683–7689.
[110] J.P. Dawson, J.S. Weinger, D.M. Engelman, Motifs of serine and threonine can drive association of transmembrane helices, J. Mol. Biol. 316 (2002) 799–805.
[111] R. Gurezka, R. Laage, B. Brosig, D. Langosch, A heptad motif of leucine residues found in membrane proteins can drive self-assembly of artificial transmembrane segments, J. Biol. Chem. 274 (1999) 9265–9270.
[112] A. Senes, D.E. Engel, W.F. DeGrado, Folding of helical membrane proteins: the role of polar, GxxxG-like and proline motifs, Curr. Opin. Struct. Biol. 14 (2004) 465–479.
[113] A. Rath, C.M. Deber, Surface recognition elements of membrane protein oligomerization, Proteins 70 (2008) 786–793.
[114] D. Thevenin, T. Lazarova, M.F. Roberts, C.R. Robinson, Oligomerization of the fifth transmembrane domain from the adenosine A2A receptor, Protein Sci. 14 (2005) 2177–2186.
[115] N. Sal-Man, D. Gerber, I. Bloch, Y. Shai, Specificity in transmembrane helix–helix interactions mediated by aromatic residues, J. Biol. Chem. 282 (2007) 19753–19761.
[116] R.M. Johnson, K. Hecht, C.M. Deber, Aromatic and cation-pi interactions enhance helix–helix association in a membrane environment, Biochemistry 46 (2007) 9208–9214.
[117] J. Fernandes, C.R. Gattass, Topological polar surface area defines substrate transport by multidrug resistance associated protein 1 (MRP1/ABCC1), J. Med. Chem. (2009).
[118] D.W. Zhang, K. Nunoya, M. Vasa, H.M. Gu, S.P. Cole, R.G. Deeley, Mutational analysis of polar amino acid residues within predicted transmembrane helices 10 and 16 of multidrug resistance protein 1 (ABCC1): effect on substrate specificity, Drug Metab. Dispos. 34 (2006) 539–546.
[119] N. Rouvière, M. Vincent, C.T. Craescu, J. Gallay, Immunosuppressor binding to the immunophilin FKBP59 affects the local structural dynamics of a surface β-strand: time-resolved fluorescence study, Biochemistry 36 (1997) 7339–7352.